UNIVERSIDADE DE LISBOA
FACULDADE DE CIÊNCIAS
DEPARTAMENTO DE FÍSICA

Ferrous Oxide Nanoparticles as liposome targeting adjuvants in mouse model melanoma chemotherapy

Nuno Guilherme Valadas da Cruz

Mestrado Integrado em Engenharia Biomédica e Biofísica
Perfil em Engenharia Clínica e Instrumentação Médica

Dissertação orientada por:
Profª. Drª. Catarina Reis
Prof. Dr. Nuno Matela

-2019-

Resumo

O melanoma é um cancro agressivo que pode facilmente ser confundido com nevos benignos quando nas fases iniciais de desenvolvimento. Com um diagnóstico precoce, a lesão pode ser removida cirurgicamente, mas esta camuflagem dificulta esse diagnóstico. Por isso, soluções terapêuticas para tratar melanoma em fases mais avançadas são cruciais para atingir boa qualidade de vida e taxa de sobrevivência do paciente. A terapia standard para tratar melanoma em estadios mais avançados envolve quimioterapia com Dacarbazina, um agente aprovado pela FDA em 1975, mas baixa resposta ao tratamento e taxa de sobrevivência encorajam a investigação de outras opções de tratamento.

Alternativas quimioterapêuticas, como um análogo oral da Dacarbazina, ou fármacos metálicos como a cisplatina existem, mas sem se destacarem do tratamento padrão, Dacarbazina. A combinação de agentes quimioterapêuticos pode ajudar na resposta ao tratamento, levando, contudo, a mais efeitos secundários sem melhorar a taxa de sobrevivência. Agentes imunoterapêuticos, que induzem ou fortalecem a resposta imunitária contra células tumorais, como Ipilimumab, Interferão-Alfa, Interleucina-2 e Timosina Alfa 1 obtiveram melhores resultados em termos de resposta e sobrevivência, sendo que Ipilimumab foi aprovado como um tratamento de primeira linha na Europa. Ainda assim, necessitam de monitorização de efeitos secundários para garantir qualidade de vida dos pacientes, o Interferão-Alfa e Interleucina-2 são especialmente tóxicos. Outra alternativa ainda, apelidada de terapia dirigida, ataca os caminhos de sinalização usados pelas células tumorais para crescerem e se replicarem, tendo já alguns tratamentos aprovados com um desempenho superior à Dacarbazina, como Dabrafenib e Cobimetinib. A limitação destes tratamentos reside na resistência ao fármaco que é desenvolvida ao longo do tratamento, impedindo um tratamento extenso com o mesmo agente terapêutico. Finalmente, é possível ainda combinar agentes com ações diferentes, correndo sempre o risco de aumentar a severidade ou quantidade de efeitos secundários sobre o paciente.

Qualquer opção terapêutica usada resulta invariavelmente em efeitos secundários, que podem ser minimizados através da construção de um sistema de entrega adequado. Sistemas de entrega de fármacos almejam: aumentar a aceitação de fármaco, ao aumentar a quantidade de fármaco disponível no local alvo e minimizar efeitos secundários, ao reduzir a exposição de células e tecidos saudáveis aos agentes terapêuticos. Conseguir esta administração focada em células doentes pode ser conseguida de várias formas, desde exploração das características físico-químicas das células ou tecido alvo, ou usando estímulos externos para guiar o sistema ou induzir a libertação do fármaco.

Em trabalho prévio, Cuphen, um composto de cobre e fenantrolina com efeitos de oxidação do ADN e inibição de aquaporinas, foi incorporado em lipossomas. Tanto o Cuphen livre como os liposomas com Cuphen exibiram baixa atividade hemolítica e nenhuma toxicidade *in-vivo*, mantendo ao mesmo tempo alta citotoxicidade contra linhas celulares de melanoma e cancro do cólon. Recentemente, outras formulações com Cuphen foram testadas num modelo singénico murino de melanoma, exibindo sensibilidade ao pH e debilitando seriamente o crescimento tumoral. Como as formulações prévias, estes lipossomas com Cuphen também exibiram baixa atividade hemolítica e nenhuma toxicidade *in-vivo*. As formulações desenvolvidas no trabalho mencionado baseavam-se em direcionamento passivo do sistema, explorando o efeito de Permeação e Retenção Aumentadas para facilitar a acumulação dos lipossomas, e usando o característico baixo pH do ambiente tumoral para libertar o fármaco.

O apelo dos lipossomas como sistemas de entrega de fármacos advém da sua flexibilidade: vesículas lipídicas, constituídas por uma ou mais bicamadas lipídicas separadas por meios aquosos, torna estes sistemas compatíveis tanto para a incorporação de compostos hidrofílicos como hidrofóbicos. Além disso, a própria composição lipídica das vesículas pode ser feita à medida da utilização, sendo possível,

por exemplo, alterar a rigidez, sensibilidade ao pH e tempo de circulação destes sistemas O processo de produção dos lipossomas pode também ser ajustado para obter lipossomas de um determinado diâmetro, aumentando ainda mais a flexibilidade deste sistema.

Neste projeto, nanopartículas de óxido de ferro foram incorporadas em lipossomas sensíveis ao pH com Cuphen, para adicionar direcionamento físico à formulação. A produção dos lipossomas foi feita pelo método de desidratação e rehidratação, com uma composição lipídica baseada no trabalho prévio do grupo de investigação, que como mencionado obteve um sistema de entrega de Cuphen funcional no modelo animal, sem toxicidade. O direcionamento magnético serviria para aumentar a retenção dos lipossomas de longa circulação nos locais tumorais, e consequentemente melhorar a resposta ao tratamento ao disponibilizar mais Cuphen, mais rapidamente, às células-alvo. A utilização de magnetossomas em aplicações médicas tem visto alguma investigação: sistemas de imagem e terapia, chamados de teranósticos, podem explorar a versatilidade dos lipossomas e a sensibilidade das nanopartículas de óxido de ferro a campos magnéticos, sendo que as partículas tanto são um bom contraste de Ressonância Magnética como podem ser usadas para despoletar a libertação do fármaco.

Para produzir as nanopartículas de óxido de ferro, foi necessário encontrar um método documentado que produzisse nanopartículas biocompatíveis e solúveis em água de forma simples e rápida, visionando uma facilitação de uma possível ampliação da produção. Um método fácil, de um passo, assistido por microondas foi usado para produzir nanopartículas de óxido de ferro revestidas com Dextrano, conseguido ao modificar um processo documentado com um revestimento que, segundo a literatura, permitiria produzir partículas com características semelhantes às do processo original, mas reduzindo a quantidade de passos necessários na produção. O revestimento das nanopartículas serve tanto para aumentar a biocompatibilidade das mesmas como para reduzir a agregação. As nanopartículas assim produzidas eliciaram uma resposta hemolítica inferior a 4% e não interferiram com a atividade citotóxica do Cuphen. A citotoxicidade das nanopartículas de óxido de ferro, Cuphen e combinação de nanopartículas com Cuphen foram avaliadas pelo teste colorimétrico MTT, onde um composto amarelo é metabolizado pelas células viáveis em cultura para um composto púrpura, quantificável por espectrofotometria.

A validação do método de produção de magnetossomas foi conseguida através de um teste de centrifugação, onde lipossomas com Cuphen e magnetosomas com Cuphen foram expostos a um ciclo curto de centrifugação numa centrífuga de bancada. Segundo o trabalho previamente executado pelo grupo de investigação, os lipossomas com Cuphen com um diâmetro inferior a 200 nm não precipitam quando submetidos a um ciclo de centrifugação de 15,000 × g durante 30 minutos. necessitando no mínimo da aplicação de 250,000 × g durante 120 minutos. Os lipossomas com Cuphen não precipitaram, enquanto os magnetosomas com Cuphen formaram um precipitado, com 59 e 80% do lípido total para magnetossomas de 170 e 270 nm, respetivamente., Foi também verificada uma redução da eficiência de incorporação do Cuphen nos magnetossomas: 59 e 66% para magnetossomas de 170 e 270 nm, respetivamente, comparativamente ao valor obtido para lipossomas de Cuphen (100 e 88% para 170 e 270 nm, respetivamente) A quantificação do teor de lípido e Cuphen nas formulações desenvolvidas foi baseada em métodos colorimétricos.

Os magnetossomas também foram testados em termos de atividade hemolítica, exibindo atividade abaixo dos 5%, sendo por isso considerados seguros para administração intravenosa. Para validar as propriedades magnéticas dos magnetossomas, foi desenhado um teste *in vitro* de magnetismo, onde um volume da suspensão dos magnetossomas foi colocado numa placa e exposto ao campo de um íman permanente de Neodímio-Ferro-Boro durante tempos diferentes. A concentração de lípido e Cuphen iniciais bem como nas zonas sobre o íman e opostas ao íman foram quantificadas. De facto, os magnetossomas exibiram qualidades magnéticas: a exposição a um campo permanente resultou num

aumento de 31% da concentração de Cuphen por cima da zona do íman, ao fim de 19 horas. Contudo, não se observaram variações em termos de concentração de lípido sobre as mesmas áreas em estudo. Para além disso, quando o teste foi repetido com Cuphen na forma livre e partículas de óxido de ferro não incorporadas, não se obtiveram os mesmos resultados que com os magnetossomas.

No futuro, métodos de quantificação de ferro podem ser utilizados para conseguir avaliar diretamente a eficiência de incorporação das nanopartículas, o método de produção das nanopartículas de óxido de ferro pode ser ajustado para produzir partículas mais pequenas de forma consistente, e testes *in-vivo* podem ser conduzidos num modelo animal para confirmar se o direcionamento extra providenciado pelas nanopartículas se traduz num aumento da resposta ao tratamento.

Palavras-Chave: melanoma, partículas de óxido de ferro, lipossomas sensíveis ao pH, sistemas de entrega de fármacos, direcionamento magnético

Abstract

Melanoma is an aggressive cancer that can easily be mistaken with normal skin features, like moles, when in early stages. This complicates early diagnosis, so effective therapeutic solutions for melanoma in more advanced stages is vital for patient quality of life and survivability. If surgery is not applicable, the standard option for advanced stage melanoma is chemotherapy with dacarbazine, but low positive response and overall survival rates encourage research into other treatment options.

Any therapeutic option used will inevitably result in adverse side effects, which can be minimized by using a drug delivery system. Drug delivery systems aim to both increase drug uptake, by enhancing drug availability at target sites, and minimizing adverse side effects, by reducing healthy cell exposure to the therapeutic agents. This targeting of unhealthy cells can be achieved in different ways, from exploiting the physiochemical characteristics of the target cells or tissue, to utilizing external stimuli to guide the drug delivery system or induce drug release.

In this work, iron oxide nanoparticles were prepared and incorporated into Cuphen pH-sensitive liposomes for a further targeting delivery using external stimuli. Cuphen is a copper-phenanthroline compound with both DNA oxidising and aquaporin inhibition effects and it has been shown promising results in melanoma cell lines using liposomal formulations. Now, a one-step microwave assisted method was used to produce Dextran coated iron oxide nanoparticles, which elicited a low haemolytic response and did not interfere with Cuphen's cytotoxic activity. The resulting magnetosomes were guided to a target area via a magnetic field: exposure to a permanent magnetic field resulted in an increase of Cuphen concentration over the magnet area. However, there was not a significant increase in lipid concentration over the magnet area when compared to free Cuphen. Further studies must be performed.

As future strategies, iron quantification methods can be employed to directly quantify the iron oxide nanoparticles' incorporation efficiency and the iron oxide nanoparticle production method can be adapted to consistently make smaller particles, and, finally, *in-vivo* tests can be conducted in an animal model to confirm whether the added targeting capabilities translate into an increase in treatment response.

Keywords: melanoma, iron oxide nanoparticles, pH-sensitive liposomes, drug delivery systems, magnetic targeting

Abbreviations

Abbreviation	*Description*
CHEMS	cholesteryl hemisuccinate
Cuphen	Cu^{2+}(1,10-phenanthroline)$_3$
EPR	Enhanced Permeability and Retention
Dex-70	Dextran - 70
DLS	Dynamic Light Scattering
DMPC	Dimiristoyl phosphatidyl choline
DMSO	Dimethyl sulfoxide
DNA	Deoxyribonucleic Acid
DOPE	Dioleoyl phosphatidyl ethanolamanine
DSPE-PEG(2000)	Distearoyl phosphatidyl ethanolamine covalently linked to to polyethylene glycol (2000)
HEPES	Hydroxyethyl piperazineethanesulfonic acid
IC_{50}	Half maximal inhibitory concentration
ICP-MS	Inductively coupled plasma mass spectrometry
I.E.	Incorporation Efficiency
IL-2	Interleukin-2
IFN	Interferon
IONPs	Iron Oxide Nanoparticles
kcts	Kilo counts
MTT	Dimethylthiazolyl diphenyltetrazolium bromide
MRI	Magnetic Resonance Imaging
MW	Molecular Weight
MWCO	Molecular Weight Cut-Off
NdIB	Neodymium – Iron – Boron
PBS	Phosphate-buffered saline
PE	Phosphatidylethanolamine
PEG	Polyethylene glycol
PdI	Polydispersity Index
SPIONS	Superparamagnetic Iron Oxide Nanoparticles
TEM	Transmission Electron Microscopy
UV	Ultraviolet
UV/Vis	Ultraviolet/Visible

Acknowledgements

"No man is an island entire of itself; every man

is a piece of the continent, a part of the main;"

- John Donne

I'd like to thank everyone who made this work possible, only with the support and collaboration of others was this project possible.

Prof. Dr. Lia Ascensão, who kindly supplied her TEM imaging expertise to produce the images presented in this thesis;

Prof. Dr. Adília Charmier, Dr. Manas Sutradhar and Dr. Tannistha Roy Barman, who allowed me access to the microwave reactor, taught me how to use it, and were always available to answer any questions or help solve any problems related to the equipment;

Dr. Manuela Gaspar, who shared her extensive knowledge on liposomes, and was always there to help steer the project into the right direction. Her advice and expertise were paramount in helping this project move forward;

Jacinta Pinho, with whom I had the pleasure to work closely with during this project, she's one of the most diligent, available, friendly and organized people I've ever met. She helped me gather my bearings in the lab and was an impeccable lab partner;

Prof. Dr. Catarina Reis, who I've been lucky enough to have met in my Batchelor's internship, and who has taught me a lot about what it means to be a researcher, and the realities of being a part of the scientific community. She's been my inspiration to keep working and learning, there's no one else I'd rather have as my supervisor;

Prof. Dr. Nuno Matela, who didn't hesitate to be my supervisor in this project: his insight, availability and instinct made for very productive brainstorming sessions;

My great friends for their unwavering companionship and complicity , especially to: Jorge, who helped me in but a moment's notice when I desperately needed it, and with whom and another of my best friends, Miguel, shared some of the best times I've had during the entire time I've been in Lisbon; Euclydes, Fábio and their mother Jessika, who took me in as one of their own for this past year, saving me from long and exhausting trips between my hometown and the lab during this crucial step in my education.

Lastly, I'd like to thank my family for their support over these past seven years, with special thanks to:

My father Paulo, my twin brother Duarte and my older brother Tiago: the work we did together as re-enactors over the years was both a welcome distraction from the pressure of university and a satisfying job;

My aunts: Lena, that with her financial aid made sure I could finish my degree, and Luísa, who opened her home and took me in. She, along with my sister Joana and my cousin Maria, supported me and helped me overcome some of the greater emotional hurdles I've experienced during this stage of my education.

I dedicate this thesis to my mother, Paula, who even in her illness still did everything she could for her children. Every day her constant fight earned her was a blessing to all of us. May she rest in peace.

Contents

1. Introduction

1.1. Motivation

Melanoma is a common, aggressive cancer derived from the malignant transformation of melanocytes, normally tied to UV exposure that typically starts in the largest human organ, the skin, though it can very rarely manifest itself in the eye or mucous membranes. In its cutaneous form, it assumes the likeness of moles and other skin features [1], camouflaging it until a larger, more obvious lesion is formed, or until a trained eye recognizes it. If the patient or the physician suspect of a mole or other skin feature, a biopsy might be conducted, to confirm the nature of the tissue.

Figure 1.1: Superficial Spreading Melanoma lesions. Irregular edges are a key telling sign of a possible cancerous lesion.

Upon finding a thick (1 to 4 mm) tumour, a sentinel lymph node biopsy follows, to evaluate whether the cancer has already metastasized. To find the sentinel lymph node, one must use blue dye and a radioactive tracer, following it to the first lymph node it reaches, removing it immediately and sending it to analysis. This works because lymph nodes have valves that stop backflow, making lymph flow in one way only. This means there will always be a node closest to the tumour, being the node responsible for draining it, and therefore susceptible to capture its cells. For an invasive, metastatic manifestation, surgery stops being the main therapy, and alternatives like chemo-, immuno- and targeted therapy come into play.

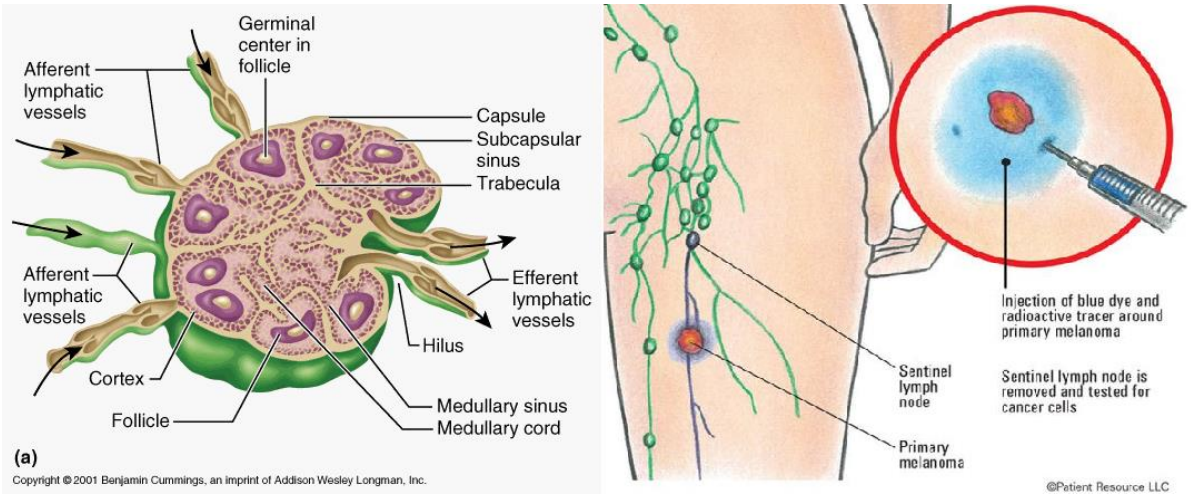

Figure 1.2: Lymph node anatomy and sentinel lymph node biopsy

Chemotherapy allows for a systemic reach over the cancerous sites and cancerous cells in circulation, though it tends to affect healthy tissues as well, leading to side effects. Furthermore, chemotherapy for cancer treatment has a fairly narrow range for dose safety and effectiveness, meaning that the window

between an ineffective treatment and a life-threatening one is small [2]. Reducing the side effects and the administered dose while still achieving an effective treatment can come via targeting. Targeting can be achieved in different ways [3]:

- **Direct:** literal, via the usage of injections, lotions or other topical applications;
- **Passive:** exploiting pre-existing characteristics of the diseased tissue, like vasculature and lymphatic drainage defects;
- **Physical:** using physical phenomena like magnetic fields, ultrasound, pH to guide and/or release the drug;
- **Active:** based on specificity towards certain overexpressed ligands in the target tissue or cell.

There are challenges in such an approach, since new formulations must be tailored to the specific characteristics of the target tissue and, given that we still don't know much about the pharmacokinetics, biodistribution and toxicity of most targeting systems, they must be evaluated as separate entities, studied one by one until the theoretical body of knowledge catches up. This means that, even when a known drug is used, both the carrier and drug-carrier combination need profiling to assure that in optimizing drug intake we're not compromising other tissues down the line, as the novel treatment is metabolised and excreted. For instance, one must consider [4]:

- **Carrier capacity and drug potency:** in order to avoid toxicity due to excessive carrier administration, drug incorporation must be as high as possible;
- **Drug – carrier compatibility:** the drug must be able to preserve their physicochemical properties during their incorporation to the selected carrier, and remain associated with the carrier long enough to reach the target tissues;
- **Carrier biocompatibility:** the carrier should be metabolized and/or excreted effectively enough that any possible side effects of its administration are reduced when compared to the free drug.
- **Drug release rate:** the drug must be able to dissociate from the carrier in such a way that a therapeutic concentration of it is maintained in the target tissues, since a slow release might result in lower effectiveness, and a rapid release might not be an improvement over the free drug.

Liposomes as drug carriers are versatile and have been extensively studied, being able to passively target the incorporated material when administered parenterally [5]. To fulfil this, one must increase their circulation time in order to, via defective endothelium and insufficient lymphatic drainage of tumours, they can accumulate in the tissue and, relying on normal cell digestion or pH activation to break these carriers apart, release their contents.

1.2 Objectives

The present work had two major goals:

- Production of water soluble, biocompatible, superparamagnetic Iron Oxide Nanoparticles (IONPs), in a one-pot and one-step fashion;
- Incorporation of these nanoparticles in a delivery system loaded with a cytotoxic compound enhancing the targeting to solid tumours by applying a magnetic field over the target.

To pursue these goals, a set of sub-objectives were set:

- Review existing processes of IONP production, and choose a base procedure that is known to produce water soluble, biocompatible, superparamagnetic particles;
- Attempt to modify this base procedure, making it as quick and facile as possible;
- Verify that the modified procedure still produces IONPs with the desired size and biocompatibilty;
- Choose a delivery system to incorporate the IONPs;
- Choose a compound with cytotoxic potential towards melanoma cell lines;
- Test whether the IONPs interfere with the elected cytotoxic compound on melanoma cells viability;
- Design nanoparticulate structures that can carry both IONPs and the selected cytotoxic compound;
- Observe whether the new nanoparticulate structure can be magnetically guided.

2. State of the Art

2.1 Melanoma Treatment

Surgery is the mainstay option for early stage melanoma [6], though the procedural details vary depending on its features: the larger the tumour (according to Breslow's thickness measurement), the bigger the safety margin on the excision must be [7]. Melanoma stages range from 0 to 4 and are attributed depending on the TNM classification. T stands for tumour, N for lymph nodes and M for metastasis. A brief description of the stages is as follows[8]:

- Stage 0 classifies a small tumour *in situ*, with no lymph node involvement and no metastasis;
- Stage 1 (or I) classifies a small tumour that has gone beyond the epidermis, up to 0.8mm thick with ulceration or 2 mm with no ulceration, no lymph node involvement and no metastasis;
- Stage 2 (or II) classifies any tumour larger than those in Stage 1 with no lymph node involvement and no metastasis, or a non-metastatic tumour present only in a single lymph node, with no primary tumour present;
- Stage 3 (or III) classifies large tumours that affect multiple lymph nodes, regardless of the presence of a primary tumour;
- Stage 4 (or IV) classifies any tumour that has metastasized.

When the cancer metastasizes, the prognosis is poor, and survival rates are low [9], [10], mostly because of melanoma cells' resistance to treatment. As such, several treatment options exist, from chemotherapy, to immunotherapy and targeted therapy [11] (Figure 2.1). Even with all these options, some of them showing an increase in response (reduction of tumours) comparatively to older treatment regimens, there is still a severe lack of options that allow for survival benefits [12][13].

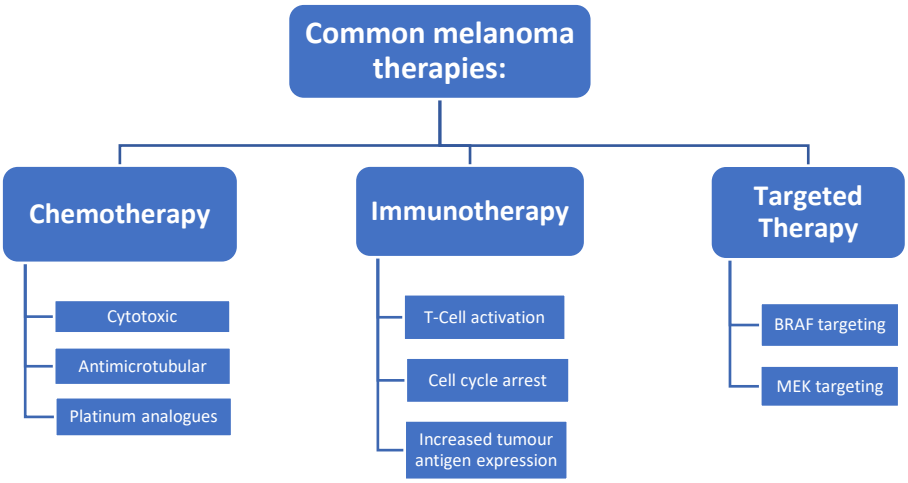

Figure 2.1: Common melanoma therapies and their main mechanisms

2.1.1. Chemotherapy

Therapy with a cytotoxic agent is the standard treatment for metastatic cancer, having its mainstay drug, Dacarbazine, been approved by the FDA in 1975. Even though it has been the custom treatment for metastatic melanoma ever since, its response ratio and overall survival benefits are still underwhelming (about 15% positive response after 6 months, OS <2% after 6 years) [14][15].

Another drug, Temozolomide, an analogue of Dacarbazine for oral administration, has shown similar performance in overall patient survival [16]. Other agents, like antimicrotubular agents, that disrupt

either microtubular assembly or disassembly, and platinum analogues like cisplatin, that bind covalently to DNA and can also work as radiosensitizers also exist. However, they show reduced response rates in Phase II trials, or when there's a higher response rate, it's short lived [17][18]. Combining different cytotoxic agents also didn't prove more useful in increasing overall survival, and furthermore burdened the patients with added toxic side effects [13].

2.1.1.1. Potential Chemotherapeutic Agent: Cuphen

The therapeutic agent used in this work is Cuphen, a Cu^{2+}-phenantroline compound that has both a DNA oxidizing action as well as an aquaporin inhibition effect [19]. Aquaporins are a surface protein estimated to facilitate tumour growth due to their key function as water and small solute transporters, helping them maintain osmotic pressure. In tumours, where they're overexpressed, they can also facilitate infiltration, cell migration and angiogenesis [19][20][21]. Nave *et al* incorporated Cuphen in liposomes and observed a preservation of *in vitro* cytotoxic effects against murine melanoma and colon cancer cell lines (B16F10 and C26, respectively), as well as human cell lines: epidermal carcinoma (A431) and melanotic neuralectodermal tumour (MNT-1). Moreoverthe absence of *in vivo* toxicity when administered parenterally, demonstrated this liposomal formulation as a potential chemotherapeutic option for cancer treatment [19].

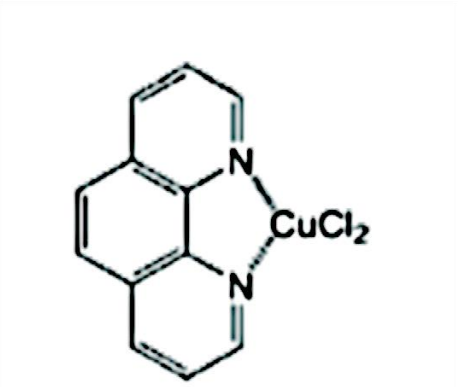

Figure 2.2: Structure of the organic-inorganic compound CuphenCl2

Recently, Jacinta and colleagues have tested Cuphen nanoformulations in a murine melanoma model. One nanoformulation using the same lipid composition as the one selected in this study, attained an 87% incorporation efficiency of Cuphen into the liposomes. That formulation exhibited pH sensitivity and significantly stunted tumour growth in a syngeneic murine melanoma model [22].

2.1.2. Immunotherapy

Agents that bolster immune response against tumours are immunotherapeutic. Cancer cells are able to avoid both cellular death and targeting by immune cells, such as T cells [7]. However, melanoma seems to be a very immunogenic cancer [23], and tumour infiltrating lymphocytes, that help the immune system in recognizing and responding against cancer, have been proved to cause a positive response in people with malignant melanomas [24]. Therapy with Ipilimumab, Interferon-Alpha, Interleukin-2 and Thymosin Alpha 1 are the most common [25].

Ipilimumab is a monoclonal antibody that blocks CTLA-4 receptors. This T-cell surface protein tells it when to become inhibited, and blocking it increases T-cell activation. The treatment saw enough improvement in survivability compared to the standard chemotherapy (Dacarbazine) treatment to be approved as a first line treatment in Europe in 2013 [26].

Interferons (IFN's) are cytokines, signalling molecules meant to trigger an immune response against viruses, tumours and microbes. They get their name because they interfere with virus replication, acting as a vaccine against viral infection. Their antitumoral activity derives from the IFN's ability to arrest the cell cycle, besides increasing T-cell activity and differentiation [27]. Unfortunately, this treatment comes with severe toxicity, and though it has shown good performance when compared to standard chemotherapy, extensive side effect management is required to maintain some quality of life for the patient [28].

Interleukin-2 (IL-2) is another cytokine with antitumoral effects [29], approved by the FDA for treatment of metastatic melanomas in 1998 [7]. Besides being a T-cell differentiator and growth factor, it also bolsters T and NK-Cells' cytolytic activity, thus achieving its antitumoral activity [30]. Full remission is possible on a very small subset of patients (70% of the full responders, considering only 5-10% of treated patients fully respond to treatment [31]), though biomarker activity assays need to be conducted to avoid serious side effects, like vascular leak syndrome [32]. Vascular leak syndrome describes an increase in vascular permeability, resulting in widespread oedema and organ failure, occurring in patients treated with either IL-2 or IFN-α [33].

Thymosin Alpha 1 is a peptide that achieves its antitumoral activity via an increase of tumour antigen expression, T-cell differentiation, and increase of cytokine production, such as Interferons and Interleukins [34][35]. In a 2010 Phase II study, its effectiveness when combined with IFN-α and Dacarbazine was tested, showing a threefold increase in treatment response, but a limited survival benefit [36].

2.1.3. Targeted Therapy

Targeted therapy in melanoma bases itself on affecting mutated proteins characteristic of metastatic disease [37], mainly the BRAF, which mutated version is present in 50% of all melanomas [38] and is a part of a signalling pathway responsible for increased growth and proliferation of cancer cells [39]. Figure 2.3 shows how the signalling cascade can be triggered through various stimuli. Take special note of the left side of the representation, where the BRAF branch of the cascade is depicted: though BRAF is the most common mutation, if resistance to the inhibitor is shown, one could target and inhibit MEK 1/2, to accomplish the same downstream effect [40].

BRAF inhibitors can induce rapid recession of metastatic melanoma [41], and several drugs have been developed, with different levels of specificity towards the mutated BRAF compared to wild-type BRAF: Sorafenib, Vemurafenib and Dabrafenib [7][11].

Sorafenib, unfortunately, hasn't shown any therapeutic promise as of late, either as a monotherapy or combination therapy, albeit being the first one being studied [42].

Vemurafenib is 30 times more sensitive to mutated BRAF than to wild-type BRAF [42], and showed promise in clinical trials from Phase I, all the way to Phase III, accruing higher overall survival rates in Phase III than standard chemotherapy (Dacarbazine) [43][44].

Dabrafenib has a 100-fold sensitivity to mutated BRAF [42], approved by the FDA in 2013 and with similar targeting mechanisms and pharmacodynamics to Vemurafenib [45], and with similar results to Vemurafenib in a Phase III trial [46], outperforming standard chemotherapy in progression free survival, though an accurate overall survival was not provided due to a reduced follow-up period in this trial.

However, BRAF inhibitors are limited by development of resistance, besides a certain inconsistency in interpatient response. Furthermore, inhibiting this pathway also interferes with healthy cell function, even though ever more mutated BRAF specific inhibitors have been developed [41].

MEK targeting drugs, like aforementioned, are a way to skirt around the BRAF inhibitor resistance that will inevitably develop, since BRAF mutated cells show increased sensitivity and selectivity towards MEK inhibitors [47], even though MEK 1/2 mutations are rarer [38].The first approved MEK inhibitor drug is Trametinib, an oral MEK 1/2 inhibitor, approved by the FDA in 2013 as a monotherapy [48]. Reviewing Figure 2.3 we can see that inhibiting MEK 1 or MEK 2 will also result in stunted growth, development and proliferation of cancer cells, and it results in improved progression free survival and overall survival when compared to standard chemotherapy [40].

Cobimetinib was approved in 2015, and is also a highly specific MEK inhibitor, taken orally in conjunction with Vemurafenib [49]. In a Phase III trial, the combination has shown improvement in response rates and progression free survival compared to both placebo and Vemurafenib monotherapy [50].

Nevertheless, MEK inhibition faces the same problem as BRAF, in that resistance to inhibition will inevitably arise [48], and that BRAF inhibitor resistance acquired via exposure to treatment can also reduce response to MEK inhibitors [51].

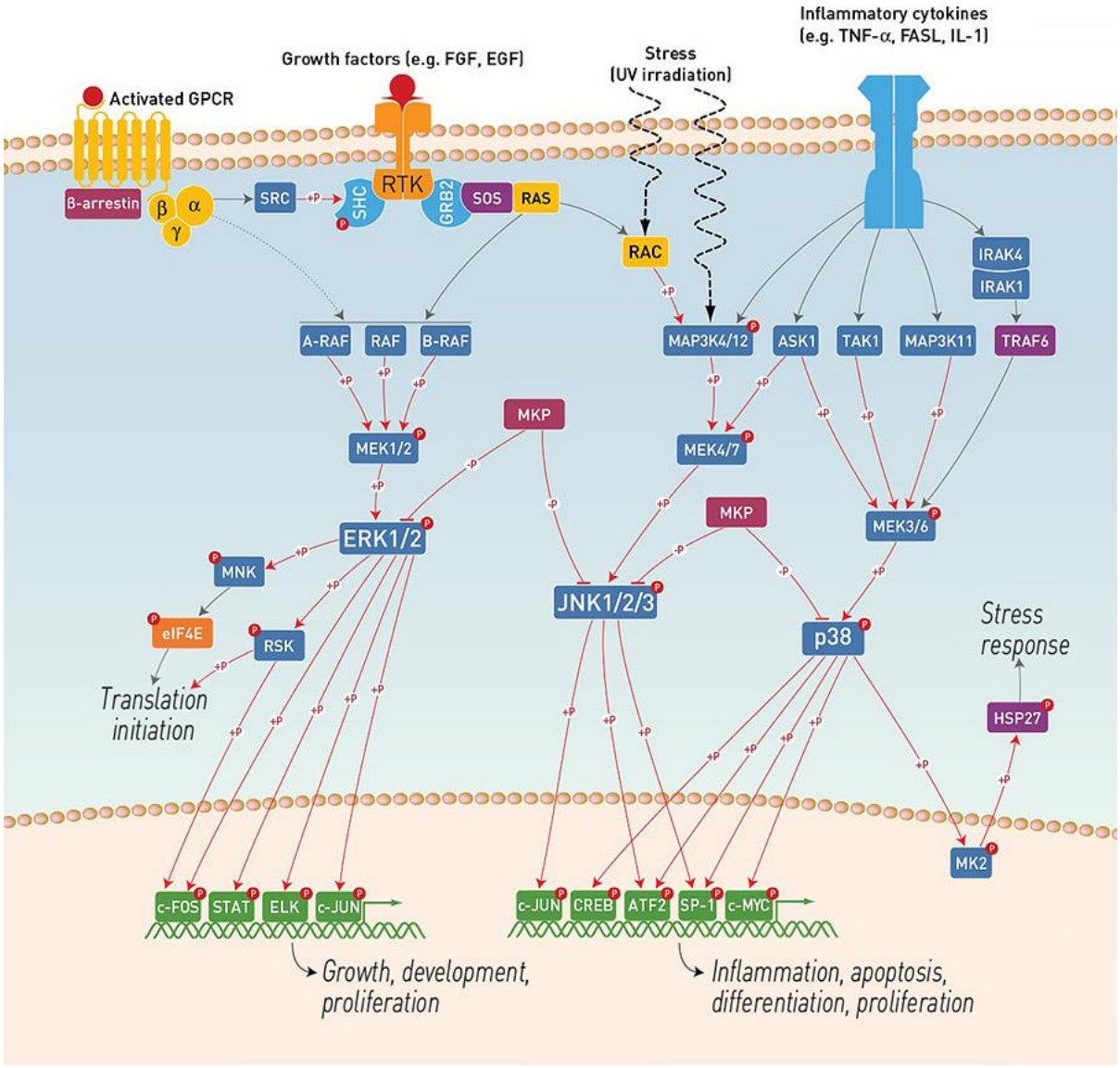

Figure 2.3: MAPK signalling pathway, extracted from [52] **(24/10/2018)**

2.1.4. Combination therapy

In an attempt to improve response and survival against a cancer with unpredictable resistances and an aggressive nature, various combination therapies have been tested, and combining therapies has become commonplace in managing this disease [11][38][41][53]. They exploit the complementary effects of chemo-, immuno- and targeted therapy. The aforementioned BRAK MEK inhibitor combination is an example of a combination therapy, shown to delay the onset of resistance and attain increased response when compared to BRAK inhibitor monotherapy [54]. Dacarbazine *plus* Ipilimumab was also studied, again achieving higher response rates and overall survival than monotherapy [55].

A Phase III trial studied the effects of a combined therapy of Cisplatin, Vinblastine, Dacarbazine, Interleukin-2 and Interferon versus high dose IFN alpha-2b, combining chemotherapy agents (DNA oxidizer, antimicrotubular agent and cytotoxic agent, respectively) with immunotherapy (both are cytokines). Good response rates and higher remission free survival were attained, but without any benefit to overall survival, and with added toxicity towards the patient when compared to high dose IFN α-2b [56]. This illustrates that, even though combining different agents can be inviting, one must consider the added toxicity risks set upon the patient.

2.2. Liposomes in Drug Delivery

Liposomes are lipid vesicles constituted by one or more concentric phospholipid bilayers enveloping aqueous compartments, as seen in Figure 2.4. These systems self-assemble when a dry lipid film is hydrated with an aqueous solution [57].

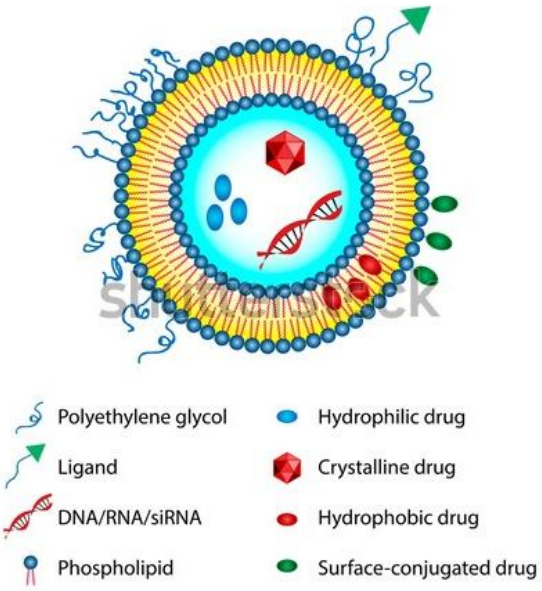

Figure 2.4: Liposome. Illustrated are their carrying capabilities, and some surface functionalization options (Stock Image)

Due to their structure liposomes are versatile carriers, with the ability to carry both hydrophilic and hydrophobic drugs, since they can be inserted on either the aqueous compartment or in the lipid bilayer, respectively, [11]. Being highly biocompatible, liposomes constitute one of the most studied and efficient drug delivery systems [58]. As previously mentioned, they are capable of transporting both hydrophilic and lipophilic drugs [59] and their surface can be modified promoting long blood circulation times, targeting specific ligands, enhancing accumulation at affected sites and consequently reducing toxic side effects [60].

Liposomes can be designed according to the compound that is meant to be incorporated, the physiological conditions of the target, and the desired application (diagnostic or treatment) [61].

One usage of liposomes is as a passive carrier. The Enhanced Permeability and Retention (EPR) effect that occurs in tumour sites can be exploited effectively: most drugs with a low molecular weight are not retained in tissues irrigated by vessels with defective endothelium and lymph drainage, however liposomes are large enough to accumulate in such areas [62]. This effect happens because when a tumour grows big enough (about 2-3 mm), angiogenesis is induced, so it continues receiving adequate levels of oxygen and nutrients. These new vessels do not possess the qualities of those in the rest of the body: they are irregular in shape, and their defective endothelium means they are leaky [63].

2.2.1. pH Sensitive Liposomes

pH sensitive liposomes are a type of liposomes that have been developed to achieve stability and long blood circulation times, while also facilitating intracellular delivery of incorporated material [64]. These liposomes destabilize in acidic conditions such as those observed around the tumour environment [65]. Coating them with polyethylene glycol (PEG) allows longer blood circulation times by stabilizing the liposome and reducing the interactions with biological milieu [66]. In addition, the inclusion in the lipid composition of pH sensitive constituents like phosphatidyl ethanolamine (PE) and its derivatives, like Dioleoyl phosphatidyl ethanolamine (DOPE) will give liposomes the intended pH sensitivity [64].

The liposomes used in the present work included in the lipid composition Cholesteryl hemisuccinate (CHEMS). Previous studies demonstrated that the presence of CHEMS was able to destabilize and release the incorporated compounds from liposomes at pH below 6.0 [22]. Poly(ethylene glycol) covalently linked to distearoyl phosphatidyl ethanolamine (PEG-DSPE) was also used in the lipid composition to achieve the aforementioned clearance time delayed [67][68].

Recently, pH sensitive liposomes have been used to reduce side effects of the incorporated compounds, by protecting them from biological milieu and thus reducing haemolytic activity in the case of problematic drugs, while maintaining cytotoxic properties [69]. They were also used to develop a theranostic systems with high serum stability and tissue uptake [70][71].

2.3. Magnetic Particles

Physical targeting systems that rely on magnetic fields aren't a novel concept. Their use to guide medical devices can be traced as far back as 1950, while magnetic particles as a contrast agent have been studied since the 60's [72]. Typically, the mode of action of a magnetic targeted system is to be injected into the blood stream and, by applying a strong magnetic field over the target tissue, the drug can be slowly released from the magnetic carrier [73]. These carriers attain their magnetism due to constituents like magnetite, maghemite and other iron oxides, nickel, cobalt and neodymium [74].

Besides their use as a contrast agent in Magnetic Resonance Imaging (MRI), magnetic particles have been researched as:

- Hyperthermia or thermal ablation agent for cancer therapy, where an oscillating magnetic field is used to create heat in target areas where the particles are [75];
- Controlled drug release systems, where the release timing and target tissue are controlled via exposure to an external magnetic stimulus, thus avoiding healthy tissue damage [76];
- Tissue engineering, for instance as scaffolding materials, so that magnetic fields can be used to mechanically stimulate cells, enhancing tissue formation and remodelling [77];
- Theranostics, so called "all in one" systems, that allow for targeting, imaging and treatment [78], possibly allowing for a "personalized nanomedicine", where one could see in real time the targeting and effects of treatment, and adjust the treatment accordingly [79];
- Lab-on-a-chip, low-cost, efficient microfluidic systems that can be used for diagnosis and monitoring [80], one such example being a malaria diagnosis device that uses magnetic resonance relaxometry for high sensitivity detection of malaria biomarkers [81];
- Drug carriers, that rely on magnetic fields to deliver their drug load to the target tissue [82].

The applications of iron oxide nanoparticles in particular have been a study subject for over 50 years [83], and several ways of producing them have arisen, ranging from physical, to chemical, to microbiological, each one with advantages and disadvantages [84]. The most common method is co-precipitation, where ferric and ferrous oxides are mixed in very basic solutions (~11 pH), and the pH is

manipulated to either facilitate nucleation (the formation of the core), or the growth of the nucleus, with more basic solutions facilitating growth and more acid solutions facilitating nucleation. Nonetheless, particles produced by this method have considerable size and shape variability, depending on the solvents used, the salts that provided the iron ions and their ratios, and other experimental parameters [85], as seen in Figure 2.5.

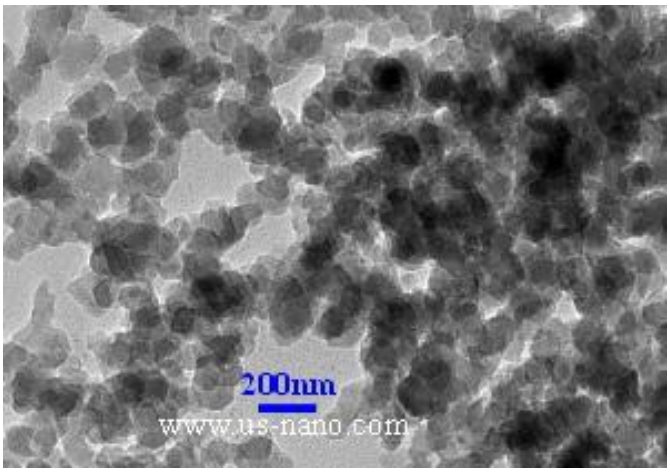

Figure 2.5: TEM imaging of commercially available iron oxide nanoparticles [86]**.**

The process used to produce SPIONS in this work does not use co-precipitation, and is based on an optimization of the production of Dextran coated SPIONS (similar to the MRI contrast agent Feridex®), using microwaves as a heat source [87]. Microwave assisted methods have existed for a couple of decades, slowly but surely being adopted as a means to reduce reaction times, starting with the usage of adapted kitchen microwaves to the dedicated equipment of today [88], where one can control pressure and temperature, besides reaction time, and even control the reaction temperature [89][90]. Dielectric heating ends up being more effective than relying on conduction and convection, and microwave reactors have allowed for higher yields, quicker and greener reactions (no fuel being burned, no oil bath to dispose of) [87].

Figure 2.6: Microwave synthesis reactors similar to the one used in this work. This equipment allows for functions such as: long reaction times, temperature setting, performing the reaction at high pressure, stirring of the contents [90]**.**

Furthermore, microwave assisted reactions allow for controlled particle size and shape, unlike co-precipitation, while sharing in its celerity [85][91]. The main principle behind this production method and most wet chemical methods is described neatly in Figure 2.7 [92]:

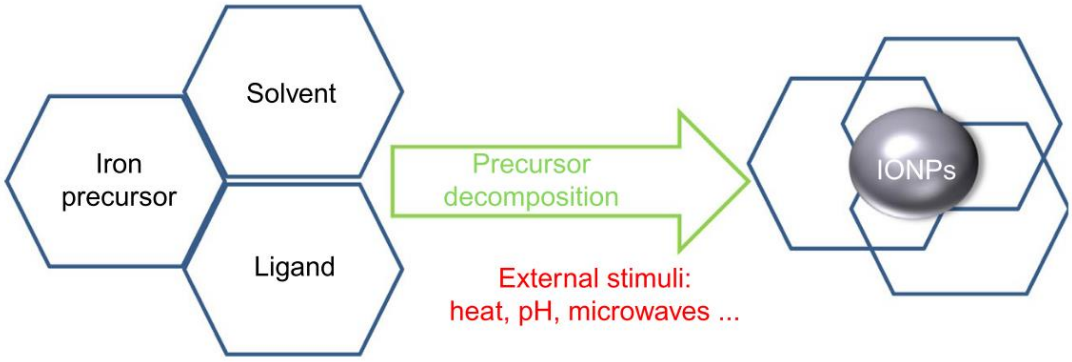

Figure 2.7: Basic principle of wet chemical production of FeO nanoparticles [92]

An Iron precursor (like an iron salt, such as the $FeCl_3$ and hydrazine mix that is used by Osborne *et al* [87]) is dissolved in a solvent, be it water or another, and, depending on the production method, a ligand is added to stabilize the particles and is usually meant to prevent particle aggregation via Van der Waals forces. Then, an external stimulus is added to lead to precursor decomposition, forming the iron cores. In one-step methods, one can use the ligand to effectively give the iron cores a coating that could increase their biocompatibility [87][93].

2.4. Liposome-SPION Delivery Systems

These mixed systems, also called magnetoliposomes, combine the carrying versatility of liposomes with the physical targeting properties of SPIONS. The points concerning liposomes apply to magnetoliposomes, since the iron oxide particles might be incorporated in liposomes, as seen in Figure 2.8: they can be included into the lipid bilayer, in the aqueous compartment, or at liposomal surface [94].

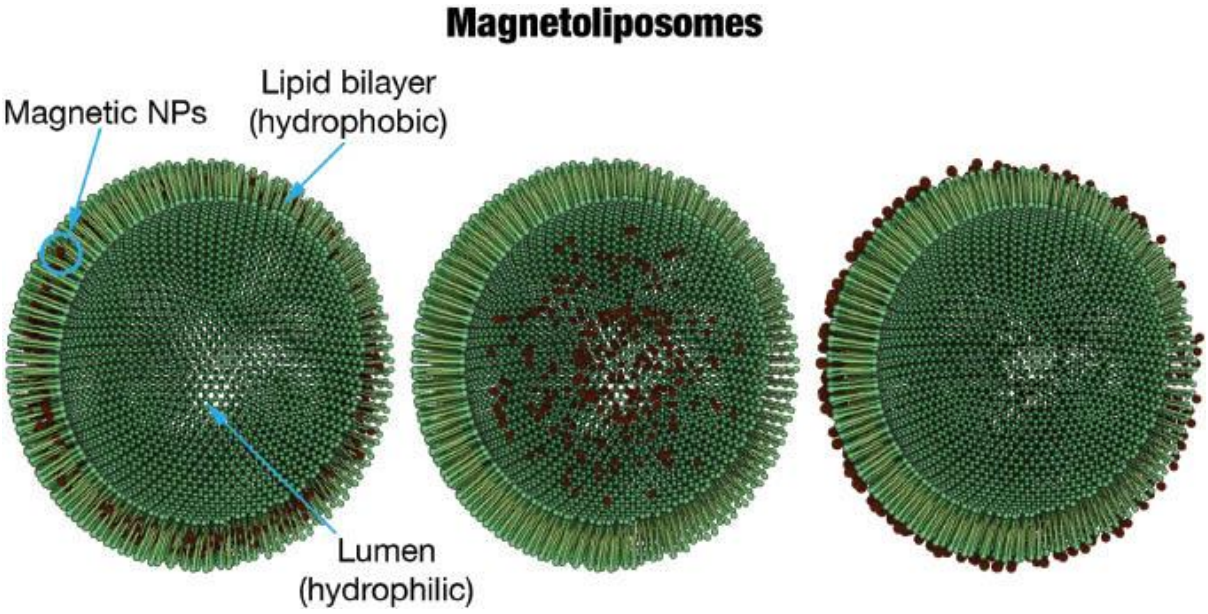

Figure 2.8: Possible magnetic nanoparticle localisations in liposomes, from [94] ***(24/10/2018)***

This means that the same procedures performed to extend blood circulation times, avoid immunogenicity and increase biocompatibility of liposomal formulations are valid for

magnetoliposomes [95]. In this sense, to effectively target the diseased tissues, the geometry of the field is crucial for achieving an optimal targeting. SPIONS, like the ones used in the present work, when combined with powerful permanent magnets (Neodymium – Iron – Boron), allow a penetration depth of 10-15 cm [96]. Magnetic implants have also been studied, and magnetic mesh or small magnets are able to be implanted near the target tissue, allowing for a less cross-sectional approach and supposedly permitting a more specific attraction of the magnetic particles [97][98].

Lately, magnetoliposomes have been studied as: MRI contrast agents to detect ischemia–reperfusion injuries, where a PEG coated liposome is loaded with also PEG coated SPIONS, and tested on a mouse liver model [99], as brain barrier penetrating doxorubicin carriers, with anti-proliferative action against B16 melanoma cells [100], as a doxorubicin carrier, folate targeting agent [101], and as a light/magnetic triggered theranostics agent [102].

3. Materials and Methods

3.1. Chemical Materials

Hydrazine Monohydrate **($H_4N_2.H_2O$)**, Dextran-70 **($H(C_6H_{10}O_5)_{70}OH$)** and Ferric Chloride **($FeCl_3$)** were obtained from Sigma (Sigma-Aldrich, MO, USA)

Dimiristoyl phosphatidyl choline **(DMPC)**, cholesteryl hemisuccinate **(CHEMS)** and distearoyl phosphatidyl ethanolamine covalently linked to to polyethylene glycol (2000) **(DSPE-PEG)** were obtained from Avanti Polar Lipids (AL, USA).

Hydroxyethyl Piperazineethanesulfonic Acid **(HEPES)** was obtained from Sigma (Sigma-Aldrich, MO, USA).

Dimethylthiazolyl Diphenyltetrazolium bromide **(Tetrazolium dye MTT)**, Dimethyl sulfoxide **(DMSO)** and $Cu^{2+}(1,10\text{-phenanthroline})_3$ **(Cuphen)** were obtained from Sigma (Sigma-Aldrich, MO, USA). B16F10 and MNT-1 cell lines were acquired from ATCC (ATCC LGC Standards), and maintained in Dulbecco's Modified Eagle's medium (DMEM) with high-glucose (4500 mg/l), supplemented with 10% fetal bovine serum and 100 IU/mL of penicillin and 100 μg/mL streptomycin.

Phosphate-buffered saline **(PBS)** was obtained from Sigma (Sigma-Aldrich, MO, USA). Blood was taken from a donor. All other reagents were of analytical grade.

3.2. Particle Production

Two types of IONPs were produced: Dextran coated, and uncoated particles.

To produce Dextran coated IONPs, 76mg of $FeCl_3$, 100mg of Dextran-70 and 8 mL of bidistilled water, along with a magnetic stirrer were introduced into a reaction vial and shaken to promote dissolution. Then, 1 mL of $H_4N_2.H_2O$ was added to the solution, turning it into a dark reddish-brown hue, given a quick shake and then inserted into the Anton Paar Microwave Synthesis Reactor ***"Monowave 300"***s reaction chamber, set at 100ºC for 10 minutes. Uncoated particles followed the exact same procedure, but no Dextran-70 was added to the initial solution.

In both particle types, a black suspension was obtained, though the uncoated particles were quick to sediment. The uncoated particles were separated from the solvent by centrifuge, at 2200g for 8 minutes. Settings were chosen such as the supernatant was clear, and the sediment would be removed from the vial. The coated particles would not sediment, and as such they were subject to dialysis using a dialysis sleeve (Medicell Int. LTD.,12000-14000 MWCO), to remove any unreacted components that remained in suspension.

After either the centrifugation or dialysis, the remaining product was lyophilized, and a black powder for the uncoated particles and a dark brown solid for the coated particles were obtained.

The process was modified to use Dextran-70 instead of Dextran-10 since, according to [103], Dextran-70 produced IONPs with comparable size (21nm mean volume diameter for both) and magnetic properties when compared to reduced Dextran-10, without needing to resort to dextran reduction, a 12h long process that would need to be repeated for every IONP batch produced. If successful, these changes would result in an even faster and facile way to produce IONPs via a microwave assisted reaction.

3.3. Particle Characterisation

After producing the particles, it became important to observe their size, so the modified procedure could be compared with Elizabeth Osborne's work [87]. Two methods were used to determine particle size: TEM and DLS, obtaining an image with the first method, and a size value with the second. The sizing of these IONPs will also matter as they must be incorporated into liposomes.

3.3.1. Transmission Electron Microscopy (TEM)

TEM, as the name implies, is a microscopy procedure where a beam of electrons is transmitted through a specimen, and then magnified and focused onto a device like photographic film or a sensor to obtain an image. The samples are ultrathin (suspensions on a grid or ~100nm sections), and higher resolution images are possible due to the smaller De Broglie wavelength of electrons when compared to photons.

Samples of both Dextran-coated and uncoated particles were prepared through the two-droplet method. The nanoparticles were resuspended in distilled water and a drop (5–10 μl) was placed and left to sit for 30–60 s on a grid coated with Formvar. After this time, the suspension was partially dried, and the grid was then washed with distilled water, any excess water removed with filter paper. Then, sodium phosphotungstate (PTA, 2%, w/v) was applied to the grid for 10 s, and the excess removed with filter paper. Finally, the grid was left to dry at room temperature for 24 h. The samples were analyzed at an accelerated voltage of 20 kV ("***Zeiss M10"***, Germany).

3.3.2. Dynamic Light Scattering (DLS)

Dynamic Light Scattering, Photon Correlation Spectroscopy or Quasi-Elastic Light Scattering is a technique that allows one to obtain the size profile of small particles in suspension, as the IONP's and magnetoliposomes produced in this work. The size values come from a relationship with the particles' Brownian motion, and is called hydrodynamic diameter (called this way because it describes how a particle diffuses in a fluid). This motion produces an image, called a speckle pattern, an interference pattern derived from the changes the particles' Brownian motion imparts on the scattering.

The hydrodynamic diameter is calculated using the Stokes-Einstein equation:

(3.1) $$d(H) = \frac{kT}{3\pi\eta D}$$

Where k is the Boltzmann's constant, T is the absolute temperature, η is the viscosity of the solvent and D is the translational diffusion coefficient. D describes how the particles diffuse in their Brownian motion, and is dependant not only on the size of the particle "core", but also its surface structure and medium ion types and concentrations [104].

The DLS (***"Zetasizer Nano S",*** Malvern Panalytical) was used to obtain the mean particle size and the PdI (polydispersity index) of the IONPs. PdI describes the homogeneity of nanoparticles ranging from 0 to a monodisperse sample up to 1.0 to a polydisperse sample. Samples were analysed at the standard scattering angle and wavelength of 175º and 663nm respectively, and 3 measurements with an automatic number of runs were taken. The samples were diluted in such a way as to get around 200 kcts on the equipment, since this way one can be certain that the sample is transparent enough that the solution or suspension will not be coloured, thus not interfering with the scattered light measurement, and that there is still enough sample to get an accurate evaluation.

3.4. Magnetoliposome Production

Liposomes were composed of a combination of DMPC:CHEMS:DSPE-PEG at a molar ratio (57:38:5), and prepared by the dehydration-rehydration method [22].

Firstly, the lipid components were weighted and introduced into a round bottomed flask and solubilized with chloroform. The solvent was then evaporated in a rotary evaporator, until a thin film is formed onto the bottom of the flask. Hydration of the film followed, using a water suspension of coated IONPs, and the resulting suspension was transferred into a vial. Any liposomes still in the flask were collected via washing with 1 mL of deionized water (Milli-Q system; ***"Elix 3 Millipore"***, Tokio).

In the case of the Cuphen-loaded liposomes, a solution of this compound was also added after the solvent evaporation and formation of a thin lipid film [19][22].

The suspension is frozen and then lyophilised overnight. Controlled rehydration occurred at 30ºC, and involved two steps: firstly, HEPES buffer pH 7.4 (10mM HEPES, 145mM NaCl) was added in an amount equivalent to 20% of the original liposomal suspension volume. After a 30-minute wait, the remaining 80% of the buffer were added, vortexed and set to rest for another 30 minutes.

Before extrusion, an aliquot of the suspension was taken for further analysis, and the remaining volume was prepared for extrusion. For that, the suspension was placed into a 10 mL vial, but not further diluted. The extruder (Lipex, Biomembranes Inc., Vancouver Canada) was washed with HEPES buffer, and the process began: the formulation was filtered under nitrogen pressure (10-500 lb/in^2), through several polycarbonate membranes of progressively smaller pore sizes, to reduce and homogenize the liposome mean size. Finally, the liposomes were submitted to a gel filtration (PD-10 column filled with Sephadex), to remove any non-incorporated IONPs or Cuphen. The resulting suspension was ready for follow-up testing.

An extensive explanation of how liposomes are prepared through the dehydration-rehydration method is present in Appendix I.

3.5. Magnetoliposome Characterisation

To characterize the magnetoliposomes, three aspects were considered: IONP incorporation, final liposome mean size, and physical targeting capabilities. To assess these characteristics, four separate procedures were conducted: a centrifuge test, a DLS assay, a lipid quantification assay and an in-vitro magnetism test. How each one was conducted and how they fit in the characterisation effort will now be described.

3.5.1. Centrifuge Test

IONPs incorporation in liposomes was verified via a centrifuge test. The liposomes used in this work do not precipitate in a benchtop centrifuge, requiring a long ultracentrifugation cycle (250,000 × g, 120 minutes) since they present mean size below 200 nm [19]. It is expected that the incorporation of IONPs in liposomes, will allow their precipitation using a benchtop centrifuge.

To conduct this test, an Eppendorf was filled with the suspension, and centrifuged in a benchtop centrifuge (***"Sigma 202 MK"***), at 15,000 × g for 30 minutes. A second sample was taken to the ultracentrifuge (***"Beckman LM-80"***), at 42,000 × g for 20 minutes, a short centrifugation cycle that allowed the comparison of both experimental conditions.

3.5.2. Dynamic Light Scattering (DLS)

In this step, DLS was used to measure the mean size and PdI of the magnetoliposomes. Running configurations were the same as IONP measurements, with standard scattering angle and wavelength of 175º and 663nm respectively, and 3 measurements per sample with an automatic number of runs each. Sample dilution followed the same precept, to get the target 200kcts.

3.5.3. Lipid Quantification

Liposomes were characterized in terms of lipid concentration using a colorimetric method described by Rouser and co-workers. In this method, inorganic phosphate is converted to phosphomolybdic acid, which is then quantitatively converted to a blue colour due to the reduction of ascorbic acid via heating [105]. Briefly, samples in triplicate containing a phosphate amount between 20 to 80 nmoL (sample volume, less than 100 µL) were pipetted into 15 mL glass tubes. In parallel, a calibration curve was constructed using a 0.5 mM sodium phosphate solution. In triplicate, phosphate amounts of 20, 30, 40, 50 60 and 80 nmoL were pipetted into glass tubes. Firstly, samples and calibration tubes are heated at 180ºC until dryness. Then, 0.3 mL of perchloric acid was added to all tubes, the tubes were capped with a marble and left for 45 minutes on the hot plate. This step converts the organic lipid phosphate into inorganic phosphate. While the 45 minutes were ongoing, a bath was prepared, with a set temperature of 100ºC. Before taking the tubes to the bath, they were left to cool at room temperature and then 1 mL of water, 0.4 mL of ammonium hexa-molibdate and 0.4 mL of ascorbic acid were added. Every tube was shaken via vortex (***"Vortex Genie 2"***, Scientific Industries), and then set in the bath for 5 minutes. Finally, the tubes were again left to cool at room temperature before absorbance levels were read at 797 nm against a blank sample in a UV-Vis spectrophotometer (***"Shimadzu UV 160A"***, Shimadzu Co.).

Samples were taken after magnetoliposome rehydration, after magnetoliposome extrusion and after ultracentrifugation (247,130 x g, 25 minutes), sampling both the pellet and supernatant. All analysed samples were diluted so the respective absorbance values would fit the calibration curve.

Curve data was fitted via linear regression, and absorbance values and sample dilutions were considered to calculate the phosphate lipid concentration, a value that could then give the total lipid concentration present in the samples. These concentrations were calculated via the following equations:

(3.2)
$$\boldsymbol{Phos/tube} = \frac{Abs - b}{m}$$

Phos/tube refers to the amount of phosphate lipid inside the sample (in µmol), *Abs* refers to the absorbance value read by the equipment, *m* and *b* refer to the appropriate values of the linear regression (y=mx+b).

(3.3)
$$\frac{\boldsymbol{Phos}}{\boldsymbol{ml}} = \left(\frac{\boldsymbol{Phos}}{\boldsymbol{tube}}\right) * \boldsymbol{Dilution} * \frac{\mathbf{1000}}{\boldsymbol{Sample}}$$

Phos/mL is the amount of phosphated lipid (in µmol) per mL of the produced liposomes, *Dilution* is the dilution factor of the sample, and *Sample* is the sample volume (in µL)

(3.4)
$$\boldsymbol{Lipid} = \left(\frac{\boldsymbol{Phos}}{\boldsymbol{ml}}\right) * \frac{\mathbf{100}}{\mathbf{62}}$$

Lipid means the total of lipid (phosphate and non-phosphate, in µmol/mL), and *100/62* is a corrective factor: the method used only accounts for phospholipid quantification that corresponds to 62 mol% of the total lipid.

3.5.4. Cuphen Quantification

To quantify how much Cuphen was incorporated in the magnetosomes, a spectrophotometric assay was used (***"Shimadzu UV 160A"***, Shimadzu Co.), at 270 nm. A calibration curve was built with Cuphen concentrations ranging from 2.5 µM to 25 µM, obtained by serial dilution of a stock solution of Cuphen at 200 nmoL/mL in Ethanol 100 %. Liposomes were destroyed by using the same organic solvent. Appropriate volumes were pipetted into eppendorfs, in triplicate. For the calibration curve 12.5 / 25 / 50 / 75 / 100 / 125 µL of the Cuphen stock solution (200 nmol/mL) were used. The sample volume for Cuphen liposomes was chosen in order to achieve absorbance values fitting the calibration curve. Next, Ethanol 100% was added to each, completing the volume to 1 mL. All samples were vortexed and the absorbances were recorded in a UV 160 Spectrophotometer (Shimadzu) against a blank sample of Ethanol 100%, using quartz cuvettes. Cuphen incorporation efficiency is given by the following expression:

(3.5)
$$\boldsymbol{I.E.}(\%) = \frac{\left(\frac{\boldsymbol{Cuphen}}{\boldsymbol{Lipid}}\right)\boldsymbol{f}}{\left(\frac{\boldsymbol{Cuphen}}{\boldsymbol{Lipid}}\right)\boldsymbol{i}} * \mathbf{100}$$

(Cuphen/Lipid)i corresponds to the Cuphen-Lipid ratio after re-hydration and before extrusion, *(Cuphen/Lipid)f* corresponds to the Cuphen-Lipid ratio after extrusion, gel filtration and ultracentrifugation, *I.E. (%)* is the incorporation efficiency, in percentage.

3.6. Biocompatibility Evaluation

It is of the utmost importance that the biocompatibility of the nanoparticles is guaranteed, since they are going to be parenterally administered. Even though they are incorporated in liposomes, once they release their contents into the target cells, the IONPs will be free, and then biocompatibility becomes an issue.

To understand whether these nanoparticles would not interfere with cells viability or blood cells, MTT and haemolysis assays were conducted.

3.6.1. MTT assay

The MTT assay is a colorimetric method to assess cell viability and proliferation. The yellow tetrazolium MTT (3-(4, 5-dimethylthiazolyl-2)-2,5-diphenyltetrazolium bromide) is reduced by metabolically active cells, in part by the action of dehydrogenase enzymes, to generate reducing equivalents such as NADH and NADPH. The resulting intracellular insoluble purple formazan can be solubilized with the aid of an organic solvent, such as DMSO and quantified by spectrophotometric means, the crystals having an absorbance peak at 570 nm.

Two MTT assays were conducted simultaneously, aiming to evaluate the biocompatibility of coated IONPs and the interaction (if any) between the chemotherapeutic agent (Cuphen) and the coated IONPs.

B16F10 cells at a concentration of 5×10^4 cells/mL were placed in 96-well plates (200 µl/well) for 24 h, in standard culture conditions (37◦C, under a 5%CO_2 atmosphere). Afterwards, culture medium was removed, and adherent cells were treated with Cuphen in free form, IONPs in free form, and the combination of both (200 µl/well).

Negative control ([ ] = 0 µM) was the cell line in the presence of culture medium. After incubation for 24 hours, the culture medium was removed from all wells (controls first, then from higher to lower concentration), and washed with 200 µl of PBS twice. Then, 50 µL of MTT reagent (0.5 mg/mL in incomplete medium) was added, followed by an incubation period of 3-4h. 100 µl of DMSO was added

to each well and “up and down” was performed with the pipette tip to dissolve the crystals. Absorbance was measured at 570 nm in a microplate reader ***(“Model 680”***, Bio-Rad, Hercules, CA).

The cytotoxic effect was evaluated by determining the percentage of viable/dead cells. Based on these values, the IC50 (concentration that reduces 50% of cellular viability) was calculated, according to an equation proposed by Hill and co-workers [106]. In order to determinate the IC50, two concentrations, X1 and X2, and the respective cell densities, Y1 and Y2, that correspond to higher or lesser than half cell density in negative control (Y0), were selected, according to the following equation:

(3.5) $$\log IC_{50} = \log X_1 + \left[\frac{Y_1 - \frac{Y_0}{2}}{Y_1 - Y_2}\right] * (\log X_2 - \log X_1)$$

Where *Y0/2*= half-cell density of the negative control; *Y1*= cell density above *Y0/2*; *X1*= concentration corresponding to *Y1*; *Y2*= cell density below *Y0/2*; *X2*= concentration corresponding to *Y2*. The IC50 was determined by linear interpolation between *X1* and *X2*.

3.6.2. Haemolysis assay

The *in-vitro* haemolysis assay, evaluates haemoglobin release in plasma (as an indicator of red blood cells lysis) following exposure to a test agent [19][107]. This procedure enables to evaluate if IONPs are safe for i.v. administration.

The first step was the collection of 25 mL of human peripheral blood, EDTA-preserved. Serum was removed by centrifugation at 1000 g for 10 minutes, and erythrocyte suspension was subsequently washed with PBS at 1000 g for 10 minutes. This step was repeated three times, discarding the supernatant each time.

Next, in a 96-well plate (non-sterile, round bottomed), serial dilutions of IONPs in PBS were made after adding 100 µl PBS in non-control wells, controls being for 100% haemolysis (200 µl water) and 0% haemolysis (200 µl PBS). One hundred µl of erythrocytes were then added to all wells and incubated for 1 hour at 37ºC. The process was repeated for the magnetosome suspension.

After incubation, the plate was centrifuged at 1000 x g for 10 minutes, and the supernatant was transferred in a new 96-well plate (round bottomed). Absorbance was read at 570 nm, with a reference filter at 630 nm through a microplate reader Model 680 (Bio-Rad, Hercules, CA), and haemolytic activity was calculated.

3.7. In-Vitro Magnetism Test

This test was designed to evaluate the IONPs ability to lead and capture the liposomes in a target area following their exposition to a magnetic field.

NdFeB Magnets were bought from José Teixeira da Rocha, Unipessoal (N38, single: 40*10*4mm, 280,2mT, stacked: 40*10*20mm, 560.9mT). 6-well cell culture plates were obtained from Greiner (***"Cellstar"***, Greiner Bio-One International GmbH).

One of the wells from the 6-well plate was filled with a magnetosome suspension and set to rest over a styrofoam surface to which the stacked magnets were affixed. The surface was set on a plate jack (***"Swiss Boy 115"***, Rudolf Grauer AG), and the 6-well plate was held by a beaker clamp. This setup allowed to separate the magnet from the plate without disturbing the suspension, and as such reduce the local magnetic field enough that a full sample could be taken. Leaving the magnet in proximity to the 6-well plate could otherwise trap part of the sample to the bottom of the plate, inducing undesired error.

Samples were taken at 1, 2, 4 and 19 hours, and both the lipid and Cuphen contents were determined. Lipid and Cuphen quantifications were done as above described.

4. Results and Discussion

4.1. Particle Characterisation

According to the work published by Osborne [87], TEM imaging of Dextran coated IONPs should show the distribution, shape and rough size of the iron cores, since Dextran would be transparent in TEM. It was also expected that the coated particles would present a smaller core and lower aggregation when compared to their uncoated counterparts. Aggregation is expected in nanoparticles, since the nanoparticles' high surface area to volume ratio means they are both especially vulnerable to Van der Waals forces [108]. Furthermore, other effects depending on the suspension medium, like charge shielding effects in saline buffers, or protein adsorption in biological medium may contribute to aggregation [109].

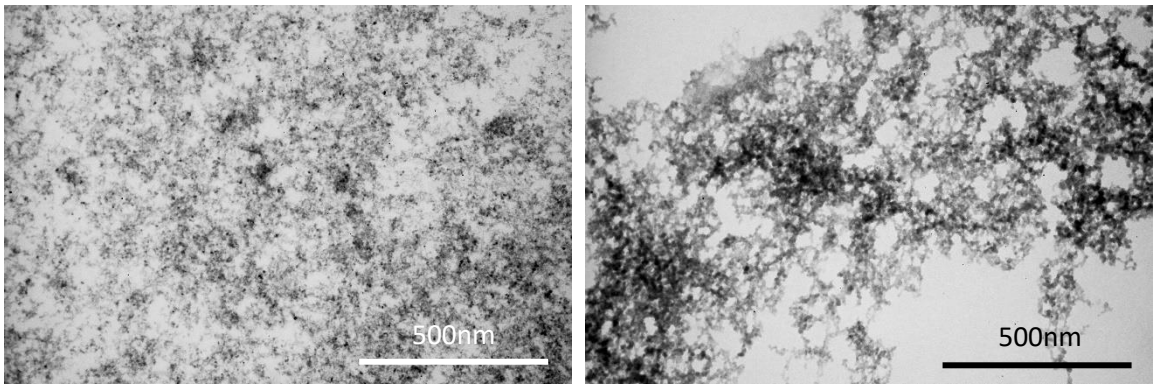

Figure 4.1: TEM images of IONPs. Left: Dex-70 coated IONPs (1st Batch). Right: Uncoated IONPs. Scale: 2.5 cm = 500 nm.

Observing Figure 4.1, the differences between coated and uncoated particles are as expected: uncoated nanoparticles present more aggregation and a larger iron core [87]. Unfortunately, there wasn't enough image resolution to observe the core morphology. The main goal of these images to confirm that coating the IONPs would result in more disperse, smaller iron cores. The exact size of these cores is obscured by both the resolution of the image and particle aggregation. That said, measuring the hydrodynamic size of the whole particle was more important than investigating the iron core morphology. This was because these particles were meant to be loaded into liposomes, and their size in suspension would largely determine the properties of the carrier.

Table 4.1: DLS sizing of Dex-70 coated IONPs, in HEPES buffer. Values expressed as average ± SD

Batch	Size (nm)	PdI
Coated IONPs 1st batch	105±2	0.238±0.009
Coated IONPs 2nd batch	170±26	0.356±0.107

Table 4.1 shows the DLS measurements of the first two batches of IONPs. They were produced in succession, for the first batch was meant as a test of the particle production process and was used up in preliminary biocompatibility tests. There is a stark difference between the hydrodynamic sizes of the first and second batches, possibly since these were produced in different microwave reaction chambers, although both chambers were the exact same brand and model. The first chamber used was sent for repairs and was as such out of order before any subsequent batches could be produced, and though the experimental setup and heating conditions of the chambers were identical, the fact is that they produced different sized IONPs.

4.2. Precipitation Test

4.2.1. Centrifuge Test

As mentioned in Section 3, the liposome formulation used is typically too light to precipitate in a benchtop centrifuge, and requires a long ultracentrifugation cycle to precipitate [19]. In the other hand, coated IONPs could be easily precipitated with a short centrifugation cycle in a benchtop centrifuge. Therefore, we could indirectly observe nanoparticle incorporation into the liposomes by measuring the amount of liposomes precipitated after a benchtop centrifuge cycle.

Table 4.2: DLS sizing and lipid contents of Cuphen magnetosomes at different stages of preparation. Size values expressed as average ± SD.

DMPC:CHEMS:DSPE-PEG (57:38:5)	**Ø (nm)**	**PdI ± SD**	**Lipid (µmol/mL)**
Initial	2384±392	1 ± 0.00	18.3
After extrusion	162±7	0.08 ± 0.01	16.0
After gel filtration	163±2	0.06 ± 0.02	9.9

Table 4.2 shows size and lipid measurements taken both at different stages of production and after the centrifugation tests. Before extrusion, the liposomes are large and polydisperse, but extrusion greatly reduced both average size and PdI, at the cost of some lipid loss. Passing the magnetosomes through the PD-10 resulted in a lower lipid concentration, but mostly due to dilution of the suspension: until the desired fraction passes through the column, buffer must be repeatedly added. The suspension obtained after column was then used for the centrifuge tests, results in Table 4.3.

Table 4.3: DLS sizing and lipid contents of Cuphen magnetosomes before and after centrifugation tests. Size values expressed as average ± SD.

DMPC:CHEMS:DSPE-PEG (57:38:5)		**Ø (nm)**	**PdI ± SD**	**Lipid (µmol/mL)**
Before centrifugation		163±2	0.06 ± 0.02	9.9 (100%)
Centrifugation 15,000 × g, 30 min	Pellet	176±2	0.06 ± 0.02	5.8 (59%)
UltraCentrifugation 42,000 × g, 20 min	Pellet	175±1	0.08 ± 0.01	5.2 (52%)

The centrifugation and ultracentrifugation tests were performed to confirm that IONPs were incorporated in liposomes. As described in methods, lower gs and time were applied to precipitate liposomes when compared to those used in the work published in Nave *et al* [19] and Pinho *et al* [22]. Comparing the results before and after the centrifugation tests, we can see both conditions led to the precipitation of larger liposomes, about the same size of the average IONP size (the batch used was the

2nd, with an average size of 170±26 nm). This suggests that IONPs were associated to liposomes and were responsible for liposomes precipitation.

Centrifuging Cuphen loaded liposomes did not quite produce a pellet. Instead of that, rather two "phases" were formed, the separation between them was so faint that a clear image of it was not possible to be taken at the time. This confirms that IONPs loaded liposomes will precipitate and form a pellet, whereas unloaded, or only Cuphen liposomes will not form a pellet, as illustrated in Figure 4.2.

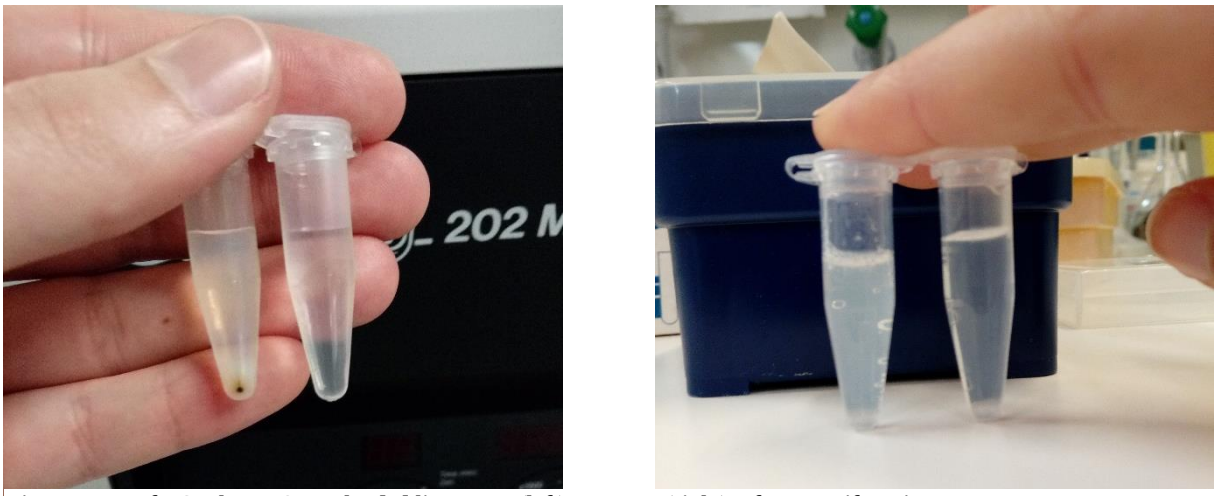

Figure 4.2: Left: Cuphen+IONPs loaded liposomes (left) Vs water (right), after centrifugation. Right: Cuphen loaded liposomes (left) Vs water (right), after centrifugation.

4.2.2. Nanoparticle Influence in Liposome Production

In order to evaluate the influence of IONPs, Cuphen liposomes were prepared in the presence or absence of IONPs and the respective incorporation parameters compared. Table 4.4 summarises the findings:

Table 4.4: Physicochemical properties of Cuphen liposomes in the presence or absence of IONPs. Values expressed as average ± SD.

DMPC:CHEMS:DSPE-PEG (57:38:5)	**(Cuphen/Lipid)f** (nmol/µmol)	**I.E. (%)**	**Ø (nm)** (PdI)	**Ø (nm) after centrifugation** (% of liposomes in pellet)
Liposomes A				
With IONPs	22 ± 1	59 ± 1	162 (<0.1)	176 (59%)
Without IONPs	26 ± 1	100 ± 2	127 (<0.1)	130 (47%)
Liposomes B				
With IONPs	25 ± 1	66 ± 1	277 (<0.1)	282 (80%)
Without IONPs	35 ± 1	88 ± 3	236 (<0.2)	249 (69%)

The Liposome B batch was made after observing that the IONPs had a similar average mean diameter to the Liposome A batch. Liposome A batch magnetosomes were bigger than liposomes loaded with only Cuphen, had a lower incorporation efficiency of the drug and only a 60% yield. A batch with larger magnetosomes would hopefully allow for higher performance in incorporation and magnetosome production: the larger liposomes were made to be around the 200 nm range, therefore bigger than the average 2nd Batch IONP size (~170 nm).

As expected, having a better fit for the average IONP left more room in the lumen for Cuphen to be incorporated (increased from 59% to 66%), but more importantly, increased the effective yield of magnetosomes (from 59% to 80%) in terms of lipid content. It should be noted that the pellets referred in the liposomes without IONPs have the same characteristics as those presented in Figure 4.2, where rather than a pellet, a sort of subtly separated "phase" formed.

With magnetosomes produced, testing proceeded towards evaluation of their *in vitro* magnetic response.

4.3. Biocompatibility Evaluation

Several MTT assays were conducted on both B16F10 and MNT-1 cell lines. The goal was both to be able to compare IONP toxicity to a known cytotoxic agent, i.e. the drug that was to be loaded alongside the IONPs into the liposomes, but also to test whether the presence of IONPs mixed with Cuphen would interfere with this drug's activity.

Table 4.5: Cell viability of B16F10 and MNT-1 after 24h incubation with IONPs. Values expressed as average ± SD.

	Cell viability (%)	
IONP Concentration (mg/mL)	**B16F10**	**MNT-1**
1	92 ± 9	85 ± 4
2	93 ± 5	102 ± 2
5	64 ± 6	80 ± 9
7.5	47 ± 4	91 ± 6

Table 4.5 indicates that the free, Dextran-70 coated IONPs, at the concentrations used, did not show any relevant loss of viability up to 2mg/mL. Cell viability was also evaluated for Cuphen exposure, and the results are presented in Figure 4.3.

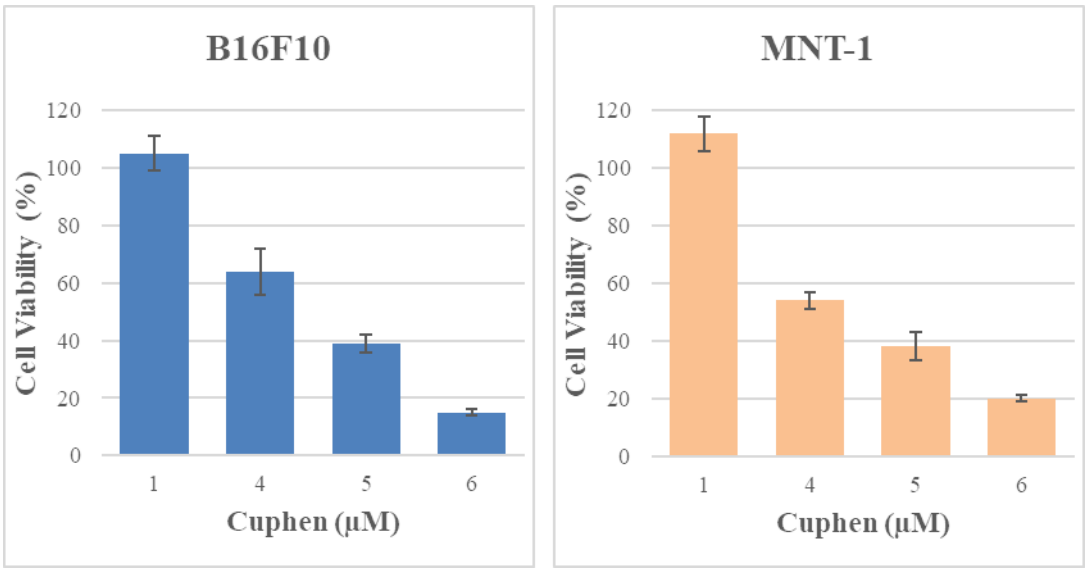

Figure 4.3: Cell viability of B16F10 and MNT-1 after 24h incubation with Cuphen. Values expressed as average ± SD.

Through the method described in Section 3, the IC_{50} of Cuphen was found to be 4.8 ± 0.3 µM for B16F10 and 4.3 ± 0.1 µM for MNT-1. The results are consistent with the determined IC_{50} values: between 4 and 5 µM. In addition, IONPs were also incubated with the two cell lines at the selected concentration in combination with Cuphen at increased concentrations ranging from 1 to 6 µM

Table 4.6: Cell viability of B16F10 and MNT-1 cells after a 24h incubation period with IONP at a concentration of 2mg/mL + Cuphen at concentrations ranging from 1 to 6 µM. Values expressed as average ± SD.

	Cell viability (%)	
Tested Formulations	**B16F10**	**MNT-1**
IONPs + 1 µM Cuphen	109 ± 4	100 ± 2
IONPs + 4 µM Cuphen	61 ± 7	62 ± 4
IONPs + 5 µM Cuphen	49 ± 4	———
IONPs + 6 µM Cuphen	15 ± 1	21 ± 2

Upon observation of the results on Table 4.6, no changes on cellular viability of Cuphen in the presence of IONPs at 2 mg/mL were observed in comparison to data in Figure 4.3. Overall the obtained results demonstrate that IONPs do not present cytotoxic properties towards melanoma cell lines and thus they may be co-incorporated in Cuphen liposomes.

Haemolytic assays were also conducted both for IONPs and Cuphen magnetosomes, results for which are in Table 4.6 and 4.7, respectively.

Table 4.6: Haemolytic effect of coated IONPs. Values expressed as average (%) ± SD.

IONPs (mg/mL)	**Haemolysis (%)**
5.0	3.4 ± 0.1
2.5	1.6 ± 0.3
1.3	0.7 ± 0.2
0.6	0.2 ± 0.1
0.3	0.0 ± 0.1

5 mg/mL was the highest concentration picked for the assay with IONPs and that from MTT assay led a cellular viability percentage of 64 and 80% after incubation with B16F10 and MNT-1, respectively Furthermore, performing serial dilutions starting at this concentration also allowed to test a concentration close to 2mg/mL. This allowed added certainty on whether the IONPs concentration chosen to be incorporated into the liposomes would be safe.

The results revealed low haemolytic activity (< 4%) for the range of concentrations tested, further reinforcing the notion that the concentration that was deemed safe, 2mg/mL, is adequate for a biocompatible application.

Table 4.7 presents the haemolytic activity for Cuphen liposomes ranging from 3.1 to 200 µM co-incorporating IONPs. The upper concentration limit was chosen to be 200 µM instead of the 750 µM used in magnetosome production since magnetosomes after gel filtration yielded approximately 200 µM Cuphen.

Results revealed low haemolytic activity (< 5%), indicating that these magnetosomes are safe for intravenous administration.

Table 4.7: Haemolytic effect of Cuphen magnetosomes. Values expressed as average (%) ± SD.

Liposomes (Cuphen + IONPs)	
Cuphen (µM)	**Haemolysis (%)**
200.0	4.6 ± 1.1
100.0	3.5 ± 0.5
50.0	1.8 ± 0.1
25.0	0.9 ± 0.2
12.5	0.4 ± 0.2
6.3	0.3 ± 0.3
3.1	0.2 ± 0.2

4.4. *In-Vitro* Magnetism Tests - validation of magnetic properties of Cuphen magnetoliposomes

4.4.1. Preliminary testing

Before starting to design the *in-vitro* magnetism test proper, some preliminary tests were conducted: should neither the IONP suspension nor the concentrated magnetosomes exhibit any magnetic response, it would require a complete overhaul of the particle production process. Both a raw suspension of IONPs and loaded magnetosomes were exposed to a NdIB magnet (560.9mT), results shown in Figure 4.4.

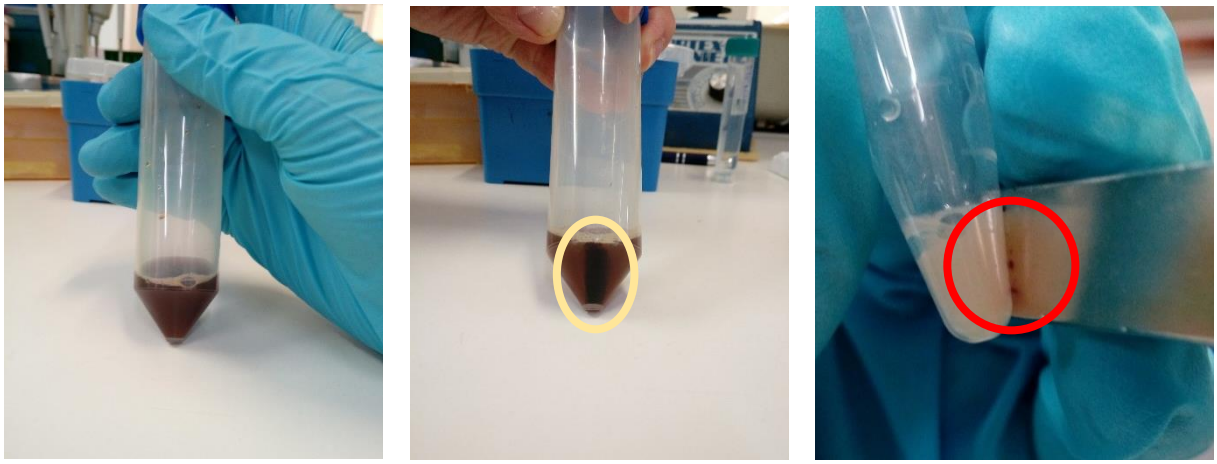

Figure 4.4: Preliminary magnetism tests. Left: Dex-70 coated IONP suspension. Centre: Dex-70 coated IONP suspension after brief exposure to a permanent magnet. Right: Magnetosome precipitate drawn to the magnet.

As exhibited, the results were highly promising: the IONP suspension reacted instantly to the magnet's presence, making the suspension clearer and resulting in a darker, concentrated area of IONPs as observed in the centre figure. The magnetosomes also responded: when concentrated they were drawn immediately to the magnet's presence. A long-term assay was then planned to further gauge liposome magnetic targetability.

The first suggestion was based on models of capillary flow [72] [110],to simulate the slower blood rates present in these superficial tumours. The self-regenerating flow would be driven through a pump, and the magnet would be placed near a target test section of tubing. The outflow would then be measured, to evaluate magnetosome retention. This was deemed to be unpractical considering the materials available in the lab and the low magnetosome volume available, therefore other, simpler options were carried out.

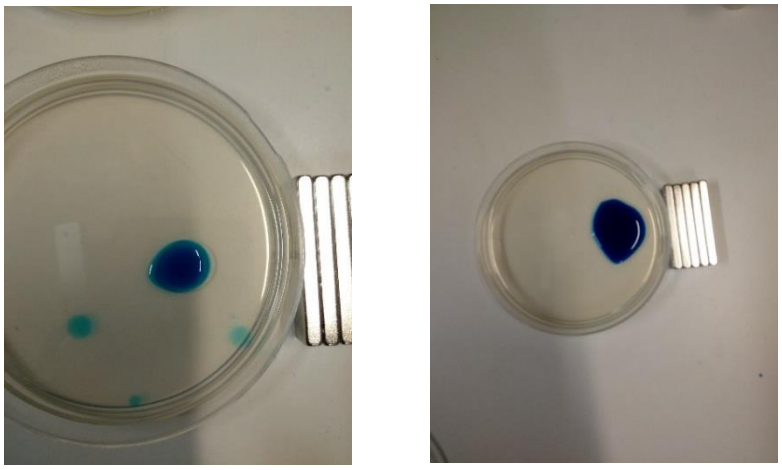

Figure 4.5: Preliminary in-vitro magnetism tests: small volume of magnetosome suspension, dyed with Blue Violet, over agar-agar. Two separate attempts after 15 mins.

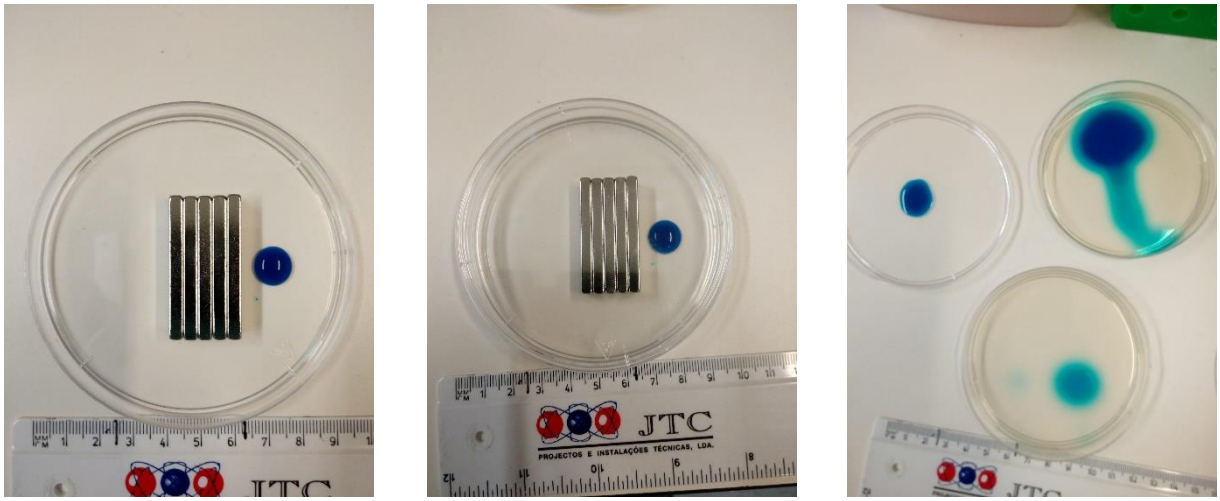

Figure 4.6: Left and Centre: Preliminary in-vitro magnetism tests: small volume of magnetosome suspension, dyed with Blue Violet, at T=0 and T=20 minutes.
Right: Aftermath of the preliminary tests. Top right well suffered spillage during handling.

Figures 4.5 and 4.6 show the first attempts at an *in-vitro* magnetism assay. Blue Violet was used as a dye, to facilitate observation of magnetosome migration towards the magnetic field. The first idea involved the use of agar-agar as a medium, as it was thought that it would allow for an easy capture of snapshots during testing, hopefully capturing the progressive formation of a colour gradient over time, as magnetosomes migrated from one end of the well towards the magnet. The small-scale assay involved just a drop over the agar-agar medium, with a magnet placed just outside the well. In sharp contrast to what was observed in the Falcon tube and the Eppendorf, no changes were visible even after 15 minutes. No deformation of the drop was observed and running the assay for a longer period of time simply resulted in permeation of suspension on agar.

Another run, this time without any medium in the well, was attempted, with the magnet placed in the well and near the drop. After 20 minutes, no changes in the drop were visible. In hindsight, this was expected: the magnetosome suspension was not a ferrofluid, due to the low concentration and high size of IONPs, and as such it wasn't reasonable to expect the drop to move in any significant way. This

meant that there was a need for a liquid medium in the wells, so that the magnetosomes were free to move inside the well, and towards the magnetic field.

4.4.2. Validation of Magnetic Properties of Cuphen Magnetoliposomes

Abandoning the drop in medium method, the magnetosome suspension was simply introduced to a small well, in a volume small enough such that the entire well was covered. This ended up being about 1.5 mL, the volume that was adopted for all the subsequent *in-vitro* magnetism assays. The experimental assay was then set up with the materials available in the lab, to minimize sample perturbation during the assay and while removing the magnet's influence. As described in Section 3, one of the wells from the 6-well plate was filled with a magnetosome suspension and set to rest over a Styrofoam surface to which the stacked magnets were affixed. The surface was set on a plate, and the 6-well plate was held by a beaker clamp (Figure 4.7)

Figure 4.7: Experimental setup for in-vitro magnetism tests.

Assays were conducted for 1, 2, 4 and 19 hours, and were all conducted separately for two reasons: the small volume inside the well reduced the number of samples that could reasonably be taken before there was insufficient coverage of the well's bottom, and to minimize perturbation of the experiment upon sample collection. Having each assay only be sampled once meant that the suspension was under the magnetic field for the entire duration of each step, and there was no risk of resuspending any magnetosomes that had already settled near the target area between samplings.

For all steps, samples were taken from: the main suspension before the 1.5 mL to fill the well were drawn, the location right over the magnet, the location opposite to the magnet, and from the remaining volume. Then, both lipid and Cuphen contents of these samples were quantified, and the concentration effect of the magnet was evaluated by comparing the Cuphen contents of the main suspension against

the contents from the sample taken from the area over the magnet. Figure 4.8 plots the results of Cuphen concentration on the magnet area over time.

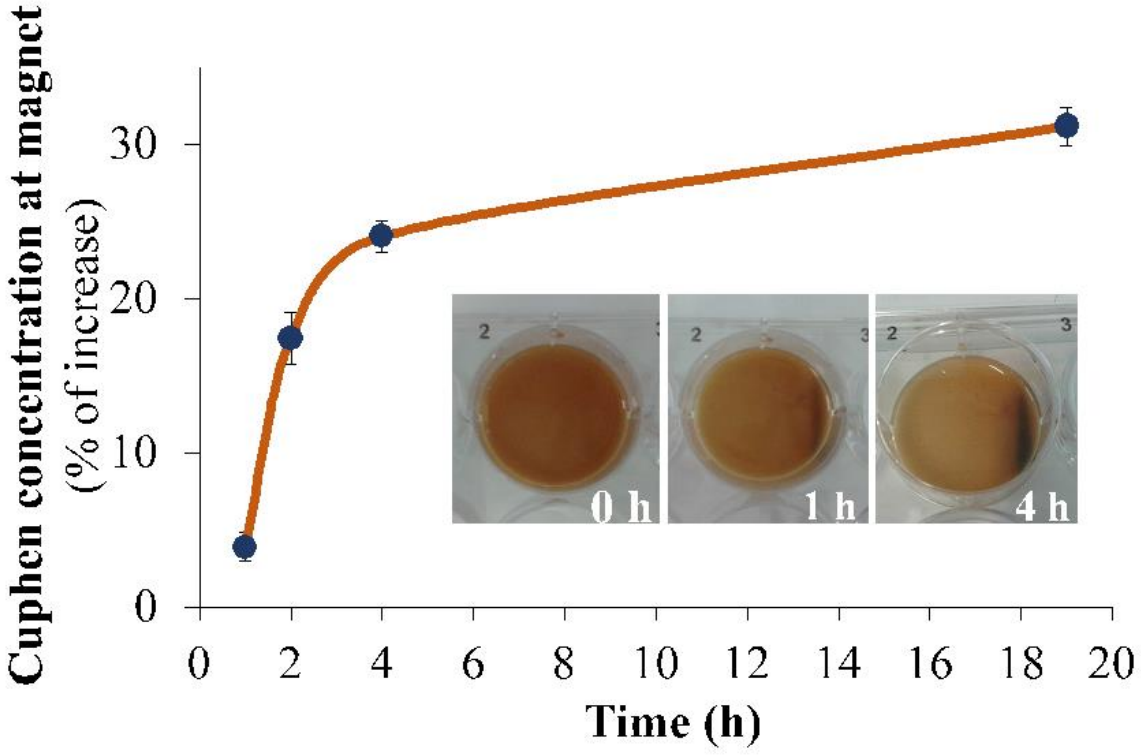

Figure 4.8: Validation of the magnetic properties of Cuphen-loaded liposomes containing FeO NPs. Graphical representation of the Cuphen increase over time. Liposomes were exposed to a magnetic field of 560.9 miliTesla for a total period of 19 h.

Over time, as the photos in Figure 4.8 reveal, the volume started becoming clearer, and a distinct dark line over the magnet formed, showing the accumulation of IONPs. It was also found that Cuphen would also increase its concentration over the magnet, causing some cautious optimism on the promise of this delivery mechanism. Lipid quantification was also conducted, results after 19h present in Table 4.9, when contrasts between the area over the magnet and the area away from the magnet are more visible.

Table 4.9: Lipid quantification of Cuphen magnetosomes after a 19h magnetism test. .Values expressed as average (%) ± SD.

Sample	**Lipid (µmol/mL)**
Initial	19.7 ± 0.3
Magnet	19.4 ± 0.4
Opposite to Magnet	20.7 ± 0.8

Unlike Cuphen, there was not an increase in lipid over the magnet compared to the location opposite to it. This was unexpected, as one would think that the magnetic field would drag the magnetosomes whole towards the magnet, so lipid concentration should increase over time, alongside with Cuphen. As the assay proceeded, no significant change in lipid concentration was found.

Two possibilities posited to explain this phenomenon were as follows:

- The dark brown agglomeration that appears over the magnet over time could be due to free IONPs present in the suspension: after all, the average nanoparticle size in the 2nd Batch was close to the average magnetosome's, so that separation by the PD-10 column would be difficult. Furthermore, the similarity in weights between free IONPs and magnetosomes (as seen in the precipitation tests), make them unreasonable to separate via centrifugation. This could be minimized by extruding the IONP suspension before making the magnetosomes or finding some way to produce smaller IONPs outright. This would not explain the increase in Cuphen concentration over time;

- There could be liposome rupture, induced by the magnetic field, which then allows the IONPs to drag along any Cuphen present in the medium. Nardoni *et al*. (2018) [111] used a magnetic field to induce drug release on liposomes with IONPs and the drug both loaded intraluminally, akin to the magnetosomes used in this work. However, the field is an oscillating one instead of a permanent one, and not enough to rupture the liposomes. Kim *et al.*(2010) [112] managed to disrupt the membrane with magnetic disks, but they attack cancer cell membranes, and as such aren't intraluminal. Again, an oscillating field is used. Podaru *et al.* (2014) [113] uses a pulsed magnetic field to create controlled magnetosome membrane disruption in intraluminally IONP loaded liposomes, and increase drug release. Membrane disruption that occurs before arriving to the magnet could explain the increase in Cuphen concentration, but no literature on disruption with permanent fields was found.

At this point, the only certainty was that the IONP modified carrier did help concentrate the drug in the area targeted with a magnetic field. Magnetosome disruption seemed unlikely in our experimental setup: literature mentions oscillating or pulsed fields as methods of increasing drug release *in situ*, but no mention of actual carrier dismantling, only controlled membrane disruption to increase permeability. Even assuming that the magnetosomes were releasing either all of its contents, or just the drug, with Cuphen being dragged along with the IONPs that were inside the magnetosome in the first case, or dragged by free IONPs that were not removed from the suspension in the second case, there lacked an explanation for the mechanism behind Cuphen's migration.

4.5. Modification Attempt

4.5.1. New Batch Characterisation

When producing the 3rd batch, experimental conditions were set to match the conditions of the 2nd batch's production, and the batch was made using the exact same microwave reactor. The recipe used was still as described in Section 3. The modified batch, made to try and reduce average IONP size, had its changes based still in Paul *et al.*'s (2004) [103] work, and instead of using 100mg of Dex-70, 244mg of the polysaccharide were used. That one change was made so that the $FeCl_3$/Dextran-70 ratio would more closely resemble the one they claim to be optimized. The previous batches used less Dextran-70 because when compared to other coating agents, like PEG, Dextran-70 is more expensive, so if similar results were obtained, it would drive IONP production costs down.

There was also the question of the size of the produced IONPs compared to literature, where the particles produced in this work appeared to be several times larger than those obtained by Osborne [87]. Some size increase was expected, since in Paul's [103] work Dextran-70 does result in larger IONPs, but the values obtained were still comparatively big. Measurements were always conducted in HEPES since that would be the intraluminal medium of the magnetosome, so it made sense to understand the particle size in that medium. To be able to directly compare the sizes of the produced IONPs with those in literature, there was a need to conduct the DLS measurements in H_2O. Table 4.10 presents the average nanoparticle sizes of both the 3rd Batch and the Modified Batch.

Table 4.10: DLS sizing of modified IONPs and the 3rd batch, in HEPES and H_2O. Values are expressed as average ± SD.

Batch	Size (nm)	PdI
Coated IONPs 3rd batch (in HEPES)	134 ± 37	0.436 ± 0.197
Coated IONPs Modified (in HEPES)	117 ± 30	0.379 ± 0.137
Coated IONPs 3rd batch (in H2O)	67 ± 23	0.204 ± 0.075
Coated IONPs Modified (in H2O)	64 ± 6	0.342 ± 0.110

The 3rd Batch, even though it was produced using the exact same procedure and equipment as the 2nd, ended up being smaller and more polydisperse (Table 4.1). Reproducing batches doesn't appear possible with the current methodology, therefore some adjustments to the procedure are necessary. One possible approach would be to change the "as fast as possible" heating setting in the microwave reactor to a fixed time period. That would have the risk of exposing the reaction mix to sub-optimal reaction temperatures for longer, leading to an overall increased reaction time and larger particles [114]. Higher microwave power settings would be necessary to reduce the heating time to a minimum.

DLS measurements in water revealed an approximate 50% reduction in average particle size when compared to measurements in HEPES, which means that the buffer could be inducing aggregation. Aggregation in buffer mediums can be mediated by charge shielding effects, where the ionic strength of the solution can reduce the electrostatic repulsion between nanoparticles [109][115]. One future experiment that can be performed to test this is a zeta potential measurement. Zeta potential serves as an approximation of the particles' surface charge, and a change in zeta potential from water to HEPES buffer would suggest that there could be charge shielding of the IONPs [108].

Figure 4.9: Modified batch after lyophilization (left) and 3rd batch after lyophilization (right)

The differences between the Modified Batch and the 3rd Batch don't end there, as Figure 4.9 illustrates, the Modified Batch produces a more compact and darker solid than the previous batches, that produced a flexible, very filamented brown solid. The solid produced by all batches was brittle. It would be interesting to understand how this change in Dextran concentration resulted in solids with different characteristics, but no literature was found on this subject.

4.5.2. FeO – Cu Interaction Hypothesis

The opposite results in lipid and Cuphen presence near the magnet, as presented in Figure 4.10 and Table 4.9, encouraged exploring the possibility of the IONPs somehow directly interacting with the drug. It was hypothesised that the IONPs could be adsorbing the copper complex, so when a magnetic field attracted the IONPs, the drug would be moved towards the magnet area too.

Guivar *et al.* (2017) [116] used functionalised IONPs to adsorb copper and lead ions present in aqueous medium, but didn't use any polysaccharide coatings. Li *et al.* (2018) [117] functionalised Fe3O4 core and Au shell (Fe3O4@Au) nanoparticles with polydopamine for Cu(II) adsorption, while Banerjee [118] functionalised IONPs with Gum Arabic. These methods take advantage of how easy it is to guide and separate magnetic nanoparticles in solution, and their better kinetics for material adsorption due to these particles' high surface area/volume ratio, often improved with specialised coating. These works suggest that, if the copper ion in Cuphen was available, this adsorption was possible.

To test this hypothesis, *in-vitro* magnetism studies with two IONP batches (3rd Batch and Modified Batch) were conducted as previously described, except the IONP + Cuphen mix wasn't incorporated into liposomes. Figures 4.10 and 4.11 show the magnetism test at 0h and 19h, respectively.

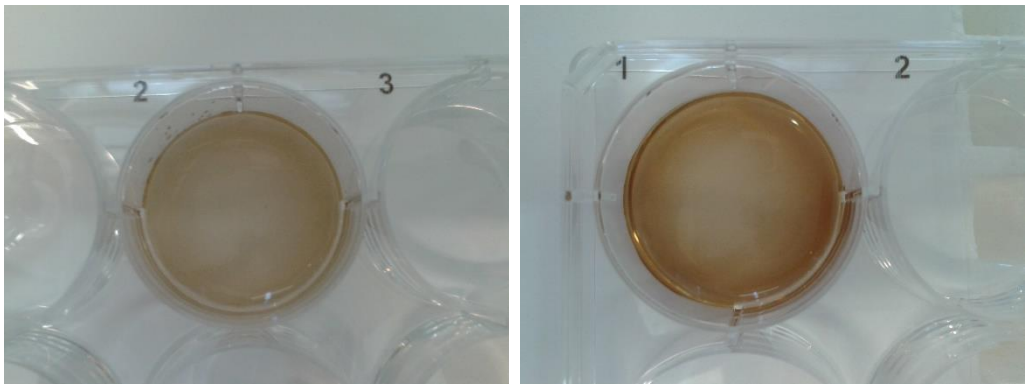

Figure 4.10: In-vitro magnetism test at T=0h with free Cuphen + IONPs produced from the 3rd Batch (Left), and the modified batch (Right).

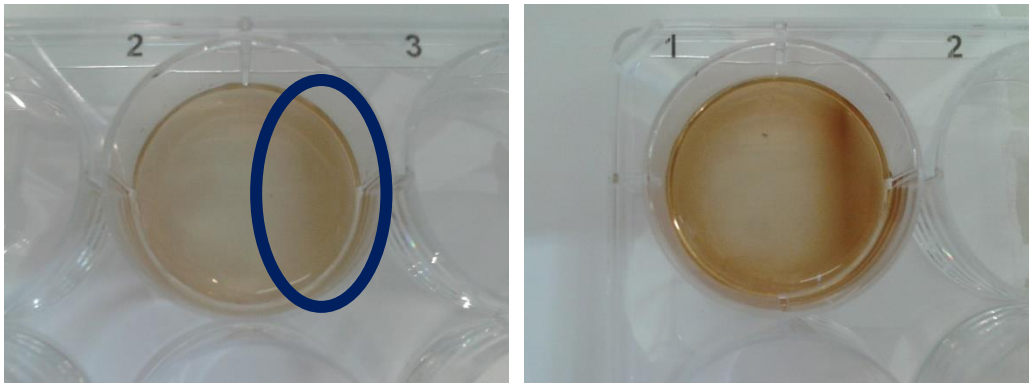

Figure 4.11: In-vitro magnetism test at T=19h with free Cuphen + IONPs produced from the 3rd Batch (Left), and the modified batch (Right).

After exposure to the magnetic field for 19h, and comparing with the images presented in Figure 4.8, one can see neither of the recent batches produces the same pronounced, dark band over the magnet area. That said, the Modified Batch appeared to perform better than the 3rd Batch, producing a clearer nanoparticle concentration band. Cuphen quantification was made to evaluate the drug's migration, results presented in Table 4.11.

Table 4.11: Cuphen quantification after a 19 h magnetism test comparing the Modified and 3rd IONP batches. Data expressed as average ± SD.

	Sample	Cuphen (nmol/mL)
Modified Free IONPs + Cuphen	Initial	1341.9 ± 23.6
	Magnet	1329.4 ± 40.2
	Opposite to magnet	1101.6 ± 18.7
3rd Batch Free IONPs + Cuphen	Initial	1146.9 ± 45.7
	Magnet	923.1 ± 14.7
	Opposite to magnet	876.6 ± 17.5

As in previous magnetism tests, the area opposite to the magnet had a lower concentration of Cuphen. But unlike what was observed before, there was no increase in Cuphen concentration in the magnet area compared to the initial suspension's concentration, even after 19h. The Modified batch did perform better than the 3rd Batch in retaining Cuphen in the magnet area, yet that performance was still inferior to the magnetosomes'. No other explanation was found to describe the results presented in Figure 4.10 and Table 4.9, further investigation is needed to better understand this mechanism.

5. Conclusions

Magnetically guided systems in medicine have seen uses from guidance of medical devices to MRI contrasts, drug delivery and theranostics. Melanoma, being an aggressive cancer with poor prognosis when in an advanced state, encourages development of drug delivery systems that improve treatment uptake and response.

In this study, Iron Oxide Nanoparticles were produced to be co-incorporated with Cuphen into liposomes, to produce novel Cuphen magnetosomes. The IONPs' production method differed from the work published by Osborne *et al.* [87], inspired by the study published by Paul *et al.*, showing that Dextran-70 coated IONPs had similar qualities to those coated with reduced Dextran-10, allowing for faster particle production by skipping the reduction process [103].

TEM imaging of IONPs found that coated particles exhibited lower core sizes and less aggregation when compared to uncoated particles. DLS measurements of different IONP batches exhibited varying mean diameters in HEPES buffer, though consistently <200nm. DLS sizing in water showed particle mean diameter <70 nm, an evidence of aggregation of IONPs when in buffer, which could hinder separation of IONPs that were not incorporated from the magnetosome suspension. Even in water, the particles were larger than the ~20nm Dex-70 coated IONPs made by Paul and colleagues, indicating that obtaining smaller particles would require adjustments to production.

Magnetosome production process was validated by centrifuge tests: benchtop centrifuging successfully precipitated >50% of the lipid in suspension into a pellet, with a Cuphen incorporation efficiency of 59%. In terms of incorporation and yield, the 270nm magnetosomes boasted higher values than the 170nm magnetosomes, an expected outcome as a larger magnetosome could incorporate more IONPs. The Cuphen magnetosomes were found to be fit for biological application: an IONP concentration that did not induce cell viability loss was chosen, and the free IONPs did not exhibit haemolytic activity (<2%). The IONPs also did not interfere with the cytotoxic activity of Cuphen, and magnetosomes had low haemolytic activity (<5%).

Magnetic targetability of the Cuphen magnetosomes was observed: *in-vitro* testing revealed a 30% increase in Cuphen concentration over the magnet area after 19h, but the mechanism behind that concentration increase remains unknown: unexpectedly, there was no lipid concentration increase over the magnet area, and tests with only Cuphen and IONPs did not replicate the results observed with the Cuphen magnetosomes.

There are ways in which this work can be expanded and improved upon, some ideas about possible alterations and future experiments will now be presented:

- Testing different microwave reaction chamber heating time and power setting combinations to maximize batch reproducibility;
- Determining the iron contents and coating efficiency of IONPs, either by using ICP-MS or a colorimetric assay that involves forming iron complexes, like the one developed by Hedayati *et al.*[119];
- Determining IONP incorporation efficiency by using either ICP-MS or a colorimetric assay, quantifying the iron present in magnetosomes;
- Reducing average particle size by extrusion or centrifugation of the IONP solution prior to liposome incorporation, or explore other coatings that result in smaller IONPs;

- *In-vivo* testing in a syngeneic murine melanoma model, where effect of the Cuphen magnetosomes on tumour growth and survival rate can be evaluated and compared with Cuphen liposomes;

6. References

[1] Melanoma Research Foundation, “Cutaneous Melanoma | Melanoma Research Foundation.” [Online]. Available: https://www.melanoma.org/understand-melanoma/what-is-melanoma/cutaneous-melanoma. [Accessed: 20-Dec-2018].

[2] The American Cancer Society, “How Is Chemotherapy Used to Treat Cancer?” [Online]. Available: https://www.cancer.org/treatment/treatments-and-side-effects/treatment-types/chemotherapy/how-is-chemotherapy-used-to-treat-cancer.html. [Accessed: 20-Dec-2018].

[3] D. Prasad and H. Chauhan, “Key Targeting Approaches for Pharmaceutical Drug Delivery | American Pharmaceutical Review - The Review of American Pharmaceutical Business & Technology,” *American Pharmaceutical Review*, 2013. [Online]. Available: https://www.americanpharmaceuticalreview.com/Featured-Articles/148744-Key-Targeting-Approaches-for-Pharmaceutical-Drug-Delivery/. [Accessed: 20-Dec-2018].

[4] T. M. Allen and P. R. Cullis, “SUPPLEMENTARY MATERIAL Drug delivery systems: entering the mainstream.,” *Science*, vol. 303, no. 5665, pp. 1818–22, 2004.

[5] T. Lammers, F. Kiessling, W. E. Hennink, and G. Storm, “Drug targeting to tumors: Principles, pitfalls and (pre-) clinical progress,” *J. Control. Release*, vol. 161, no. 2, pp. 175–187, 2012.

[6] A. Mohammadpour, M. Derakhshan, H. Darabi, P. Hedayat, and M. Momeni, “Melanoma: Where we are and where we go,” *J. Cell. Physiol.*, no. May, 2018.

[7] B. Domingues, J. Lopes, P. Soares, and H. Populo, “Melanoma treatment in review,” *ImmunoTargets Ther.*, vol. Volume 7, pp. 35–49, 2018.

[8] D. Schadendorf *et al.*, “Melanoma,” *Lancet*, vol. 392, no. 10151, pp. 971–984, 2018.

[9] C. M. Balch *et al.*, “Final version of 2009 AJCC melanoma staging and classification,” *J. Clin. Oncol.*, vol. 27, no. 36, pp. 6199–6206, 2009.

[10] E. L. Korn *et al.*, “Meta-analysis of phase II cooperative group trials in metastatic stage IV melanoma to determine progression-free and overall survival benchmarks for future phase II trials,” *J. Clin. Oncol.*, vol. 26, no. 4, pp. 527–534, 2008.

[11] H. Mishra, P. K. Mishra, A. Ekielski, M. Jaggi, Z. Iqbal, and S. Talegaonkar, “Melanoma treatment: from conventional to nanotechnology,” *J. Cancer Res. Clin. Oncol.*, vol. 144, no. 12, pp. 2283–2302, 2018.

[12] C. Garbe, T. K. Eigentler, U. Keilholz, A. Hauschild, and J. M. Kirkwood, “Systematic Review of Medical Treatment in Melanoma: Current Status and Future Prospects,” *Oncologist*, vol. 16, no. 1, pp. 5–24, 2011.

[13] S. Pasquali, H. Av, C. S. V, R. Cr, and S. Mocellin, “Systemic treatments for metastatic cutaneous melanoma (Review) SUMMARY OF FINDINGS FOR THE MAIN COMPARISON,” no. 2, 2018.

[14] S. Bhatia, S. S. Tykodi, and J. A. Thompson, “Treatment of Metastatic Melanoma: An Overview,” vol. 23, no. 6, pp. 488–496, 2009.

[15] C. Kim, C. W. Lee, L. Kovacic, A. Shah, R. Klasa, and K. J. Savage, “Long-Term Survival in Patients with Metastatic Melanoma Treated with DTIC or Temozolomide,” *Oncologist*, vol. 15, no. 7, pp. 765–771, 2010.

[16] M. R. Middleton *et al.*, “Randomized Phase III Study of Temozolomide Versus Dacarbazine in the Treatment of Patients With Advanced Metastatic Malignant Melanoma,” *J. Clin. Oncol.*, vol. 18, no. 1, p. 158, Jan. 2000.

[17] R. D. Rao *et al.*, “Combination of and paclitaxel and carboplatin as second-line therapy for patients with metastatic melanoma,” *Cancer*, vol. 106, no. 2, pp. 375–382, 2006.

[18] D. Glover, J. H. Glick, C. Weiler, K. Fox, and D. Guerry, “WR-2721 and high-dose cisplatin: An active combination in the treatment of metastatic melanoma,” *J. Clin. Oncol.*, vol. 5, no. 4, pp. 574–578, 1987.

[19] M. Nave, R. E. Castro, C. M. P. Rodrigues, A. Casini, G. Soveral, and M. M. Gaspar, “Nanoformulations of a potent copper-based aquaporin inhibitor with cytotoxic effect against cancer cells,” *Nanomedicine*, vol. 11, no. 14, pp. 1817–1830, 2016.

[20] A. Rodríguez, L. Méndez-Giménez, and G. Frühbeck, “Aquaporins in Health: New Molecular Targets for Drug Discovery,” in *Aquaporins in Health and Disease: New Molecular Targets for Drug Discovery*, 2016, pp. 103–124.

[21] I. Direito, A. Madeira, M. A. Brito, and G. Soveral, “Aquaporin-5: From structure to function and dysfunction in cancer,” *Cell. Mol. Life Sci.*, vol. 73, no. 8, pp. 1623–1640, 2016.

[22] J. O. Pinho *et al.*, “Copper complex nanoformulations featuring highly promising therapeutic potential in murine melanoma models,” *Nanomedicine*, vol. 14, no. 7, pp. 835–850, 2019.

[23] I. Lugowska, P. Teterycz, and P. Rutkowski, “Immunotherapy of melanoma,” *Wspolczesna Onkol.*, vol. 2, no. 1A, pp. 61–67, 2017.

[24] V. A. Gata, C. I. Lisencu, C. I. Vlad, D. Piciu, A. Irimie, and P. Achimas - Cadariu, “Tumor infiltrating lymphocytes as a prognostic factor in malignant melanoma. Review of the literature,” *J. B.U.ON.*, vol. 22, no. 3, pp. 592–598, 2017.

[25] C. J., S. R., Z. X.D., and C. C., “Applications of nanotechnology for melanoma treatment, diagnosis, and theranostics,” *Int. J. Nanomedicine*, vol. 8, pp. 2677–2688, 2013.

[26] C. Franklin, E. Livingstone, A. Roesch, B. Schilling, and D. Schadendorf, “Immunotherapy in melanoma: Recent advances and future directions,” *Eur. J. Surg. Oncol.*, vol. 43, no. 3, pp. 604–611, 2017.

[27] M. De Andrea, R. Ravera, D. Gioia, M. Gariglio, and S. Landolfo, “The interferon system: An overview,” *Eur. J. Paediatr. Neurol.*, vol. 6, no. SUPPL. 1, 2002.

[28] E. Jonasch, “Interferon in Oncological Practice: Review of Interferon Biology, Clinical Applications, and Toxicities,” *Oncologist*, vol. 6, no. 1, pp. 34–55, 2001.

[29] C. Krieg, S. Letourneau, G. Pantaleo, and O. Boyman, “Improved IL-2 immunotherapy by selective stimulation of IL-2 receptors on lymphocytes and endothelial cells,” *Proc. Natl. Acad. Sci.*, vol. 107, no. 26, pp. 11906–11911, 2010.

[30] W. Liao, J. X. Lin, and W. J. Leonard, “Interleukin-2 at the Crossroads of Effector Responses, Tolerance, and Immunotherapy,” *Immunity*, vol. 38, no. 1, pp. 13–25, 2013.

[31] S. A. Rosenberg, “Raising the Bar : The Curative Potential of Human Cancer Immunotherapy THE NEED FOR CURATIVE CANCER,” *Perspective*, no. 15, 2010.

[32] M. Sabatino *et al.*, “Serum vascular endothelial growth factor and fibronectin predict clinical response to high-dose interleukin-2 therapy,” *J. Clin. Oncol.*, vol. 27, no. 16,

pp. 2645–2652, 2009.

[33] R. Baluna and E. S. Vitetta, “Vascular leak syndrome: A side effect of immunotherapy,” *Immunopharmacology*, vol. 37, no. 2–3, pp. 117–132, 1997.

[34] E. Garaci *et al.*, “Thymosin alpha 1: From bench to bedside,” *Ann. N. Y. Acad. Sci.*, vol. 1112, pp. 225–234, 2007.

[35] J. Li, C. H. Liu, and F. S. Wang, “Thymosin alpha 1: Biological activities, applications and genetic engineering production,” *Peptides*, vol. 31, no. 11, pp. 2151–2158, 2010.

[36] M. Maio *et al.*, “Large randomized study of thymosin α 1, interferon alfa, or both in combination with dacarbazine in patients with metastatic melanoma,” *J. Clin. Oncol.*, vol. 28, no. 10, pp. 1780–1787, 2010.

[37] J. Poust, “Targeting metastatic melanoma,” *Am. J. Heal. Pharm.*, vol. 65, no. 24 SUPPL. 9, 2008.

[38] D. Klinac, E. S. Gray, M. Millward, and M. Ziman, “Advances in Personalized Targeted Treatment of Metastatic Melanoma and Non-Invasive Tumor Monitoring,” *Front. Oncol.*, vol. 3, no. March, pp. 1–16, 2013.

[39] A. D. Ballantyne and K. P. Garnock-Jones, “Dabrafenib: First global approval,” *Drugs*, vol. 73, no. 12, pp. 1367–1376, 2013.

[40] K. T. Flaherty *et al.*, “Improved Survival with MEK Inhibition in BRAF-Mutated Melanoma,” *N. Engl. J. Med.*, vol. 367, no. 2, pp. 107–114, Jul. 2012.

[41] A. M. Menzies and G. V. Long, “Systemic treatment for BRAF-mutant melanoma: Where do we go next?,” *Lancet Oncol.*, vol. 15, no. 9, pp. e371–e381, 2014.

[42] M. Mandalà and C. Voit, “Targeting BRAF in melanoma: Biological and clinical challenges,” *Crit. Rev. Oncol. Hematol.*, vol. 87, no. 3, pp. 239–255, 2013.

[43] K. T. Flaherty *et al.*, “Inhibition of Mutated, Activated BRAF in Metastatic Melanoma,” *N. Engl. J. Med.*, vol. 363, no. 9, pp. 809–819, Aug. 2010.

[44] P. B. Chapman *et al.*, “Improved Survival with Vemurafenib in Melanoma with BRAF V600E Mutation,” *N. Engl. J. Med.*, vol. 364, no. 26, pp. 2507–2516, Jun. 2011.

[45] T. Rajakulendran and D. N. Adam, “Bench to bedside: Mechanistic principles of targeting the RAF kinase in melanoma,” *Int. J. Dermatol.*, vol. 53, no. 12, pp. 1428–1433, 2014.

[46] A. Hauschild *et al.*, “Dabrafenib in BRAF-mutated metastatic melanoma: A multicentre, open-label, phase 3 randomised controlled trial,” *Lancet*, vol. 380, no. 9839, pp. 358–365, 2012.

[47] D. B. Solit *et al.*, “BRAF mutation predicts sensitivity to MEK inhibition,” *Nature*, vol. 439, no. 7074, pp. 358–362, 2006.

[48] E. Livingstone, L. Zimmer, J. Vaubel, and D. Schadendorf, “BRAF, MEK and KIT inhibitors for melanoma: adverse events and their management,” *Chinese Clin. Oncol.*, vol. 3, no. 3, 2014.

[49] K. P. Garnock-Jones, “Cobimetinib: First Global Approval,” *Drugs*, vol. 75, no. 15, pp. 1823–1830, 2015.

[50] J. Larkin *et al.*, “Combined Vemurafenib and Cobimetinib in BRAF-Mutated Melanoma,” *N. Engl. J. Med.*, vol. 371, no. 20, pp. 1867–1876, Nov. 2014.

[51] K. B. Kim *et al.*, “Phase II study of the MEK1/MEK2 inhibitor trametinib in patients with

metastatic BRAF-mutant cutaneous melanoma previously treated with or without a BRAF inhibitor," *J. Clin. Oncol.*, vol. 31, no. 4, pp. 482–489, 2013.

[52] "MAPK Signaling Pathway Antibodies - PT." [Online]. Available: www.thermofisher.com/pt/en/home/life-science/antibodies/primary-antibodies/antibodies-cancer-research/mapk-signaling-pathway-antibodies.html. [Accessed: 24-Nov-2018].

[53] E. A. Rozeman, T. J. A. Dekker, J. B. A. G. Haanen, and C. U. Blank, "Advanced Melanoma: Current Treatment Options, Biomarkers, and Future Perspectives," *Am. J. Clin. Dermatol.*, vol. 19, no. 3, pp. 303–317, 2018.

[54] K. H. T. Paraiso *et al.*, "Recovery of phospho-ERK activity allows melanoma cells to escape from BRAF inhibitor therapy," *Br. J. Cancer*, vol. 102, no. 12, pp. 1724–1730, 2010.

[55] C. Robert *et al.*, "Ipilimumab plus Dacarbazine for Previously Untreated Metastatic Melanoma," *N. Engl. J. Med.*, vol. 364, no. 26, pp. 2517–2526, Jun. 2011.

[56] L. E. Flaherty *et al.*, "Southwest oncology group S0008: A Phase III trial of high-dose interferon alfa-2b versus cisplatin, vinblastine, and dacarbazine, plus interleukin-2 and interferon in patients with high-risk melanoma-an intergroup study of cancer and leukemia group B, chi," *J. Clin. Oncol.*, vol. 32, no. 33, pp. 3771–3778, 2014.

[57] K. S. Ahmed, S. A. Hussein, A. H. Ali, S. A. Korma, Q. Lipeng, and C. Jinghua, "Liposome: composition, characterisation, preparation, and recent innovation in clinical applications," *J. Drug Target.*, vol. 27, no. 7, pp. 742–761, 2019.

[58] P. P. Deshpande, S. Biswas, and V. P. Torchilin, "Current trends in the use of liposomes for tumor targeting," *Nanomedicine (Lond)*, vol. 8, no. 9, pp. 1509–1528, 2013.

[59] S. Draffehn and M. U. Kumke, "Monitoring the Collapse of pH-Sensitive Liposomal Nanocarriers and Environmental pH Simultaneously: A Fluorescence-Based Approach," *Mol. Pharm.*, vol. 13, no. 5, pp. 1608–1617, 2016.

[60] J. Huwyler, J. Drewe, and S. Krähenbühl, "Tumor targeting using liposomal antineoplastic drugs," *Int. J. Nanomedicine*, vol. 3, no. 1, pp. 21–29, 2008.

[61] M. E. M. Cruz, S. I. Simões, M. L. Corvo, M. B. F. Martins, and M. M. Gaspar, "Drug Delivery Nanoparticles Formulation and Characterization," in *Drug Delivery Nanoparticles Formulation and Characterization*, vol. 191, no. January 2009, Y. Pathak and D. Thassu, Eds. Informa Healthcare USA, Inc., 2016, pp. 35–50.

[62] H. Maeda, T. Sawa, and T. Konno, "Mechanism of tumor-targeted delivery of macromolecular drugs, including the EPR effect in solid tumor and clinical overview of the prototype polymeric drug SMANCS," *J. Control. Release*, vol. 74, no. 1–3, pp. 47–61, 2001.

[63] A. K. Iyer, G. Khaled, J. Fang, and H. Maeda, "Exploiting the enhanced permeability and retention effect for tumor targeting," *Drug Discov. Today*, vol. 11, no. 17–18, pp. 812–818, 2006.

[64] S. Simões, J. Nuno Moreira, C. Fonseca, N. Düzgüneş, and M. C. Pedroso De Lima, "On the formulation of pH-sensitive liposomes with long circulation times," *Adv. Drug Deliv. Rev.*, vol. 56, no. 7, pp. 947–965, 2004.

[65] C.-J. Chul, F. C. Szoka, and C.-J. June Chu, "pH-SENSITIVE LIPOSOMES," *J. LIPOSOME Res. J. Liposome Res. Downloaded from informahealthcare.com by Univ. North Carolina*, vol. 4, no. 1, pp. 361–395, 1994.

[66] H. Karanth and R. S. R. Murthy, “pH-Sensitive liposomes-principle and application in cancer therapy,” *J. Pharm. Pharmacol.*, vol. 59, no. 4, pp. 469–483, 2007.

[67] R. Wang, R. Xiao, Z. Zeng, L. Xu, and J. Wang, “Application of poly(ethylene glycol)-distearoylphosphatidylethanolamine (PEG-DSPE) block copolymers and their derivatives as nanomaterials in drug delivery,” *Int. J. Nanomedicine*, vol. 7, pp. 4185–4198, 2012.

[68] M. M. Gaspar, O. C. Boerman, P. Laverman, M. L. Corvo, G. Storm, and M. E. M. Cruz, “Enzymosomes with surface-exposed superoxide dismutase: In vivo behaviour and therapeutic activity in a model of adjuvant arthritis,” *J. Control. Release*, vol. 117, no. 2, pp. 186–195, 2007.

[69] Y. P. Fang, P. Y. Hu, and Y. Bin Huang, “Diminishing the side effect of mitomycin c by using ph-sensitive liposomes: In vitro characterization and in vivo pharmacokinetics,” *Drug Des. Devel. Ther.*, vol. 12, pp. 159–169, 2018.

[70] Y. Duan, L. Wei, J. Petryk, and T. D. Ruddy, “Formulation, characterization and tissue distribution of a novel pH-sensitive long-circulating liposome-based theranostic suitable for molecular imaging and drug delivery,” *Int. J. Nanomedicine*, vol. 11, pp. 5697–5708, 2016.

[71] C. O. Silva, J. O. Pinho, J. M. Lopes, A. J. Almeida, M. M. Gaspar, and C. Reis, “Current trends in cancer nanotheranostics: Metallic, polymeric, and lipid-based systems,” *Pharmaceutics*, vol. 11, no. 1, 2019.

[72] A. Senyei, K. Widder, and G. Czerlinski, “Magnetic guidance of drug-carrying microspheres,” *J. Appl. Phys.*, vol. 49, no. 6, pp. 3578–3583, 1978.

[73] E. K. Ruuge and A. N. Rusetski, “Magnetic fluids as drug carriers: Targeted transport of drugs by a magnetic field,” *J. Magn. Magn. Mater.*, vol. 122, no. 1–3, pp. 335–339, 1993.

[74] U. O. Häfeli, “Magnetically modulated therapeutic systems,” *Int. J. Pharm.*, vol. 277, no. 1–2, pp. 19–24, 2004.

[75] M. Bañobre-López, A. Teijeiro, and J. Rivas, “Magnetic nanoparticle-based hyperthermia for cancer treatment,” *Reports Pract. Oncol. Radiother.*, vol. 18, no. 6, pp. 397–400, 2013.

[76] J. Barbosa *et al.*, “Magnetically Controlled Drug Release System through Magnetomechanical Actuation,” *Adv. Healthc. Mater.*, vol. 5, no. 23, pp. 3027–3034, 2016.

[77] Y. Li, D. Ye, M. Li, M. Ma, and N. Gu, “Adaptive Materials Based on Iron Oxide Nanoparticles for Bone Regeneration,” *ChemPhysChem*, vol. 19, no. 16, pp. 1965–1979, 2018.

[78] B. Sumer and J. Gao, “Theranostic nanomedicine for cancer,” *Nanomedicine*, vol. 3, no. 2, pp. 137–140, 2008.

[79] T. H. Kim, S. Lee, and X. Chen, “Nanotheranostics for personalized medicine,” *Expert Rev. Mol. Diagn.*, vol. 13, no. 3, pp. 257–269, 2013.

[80] C. D. Chin, V. Linder, and S. K. Sia, “Commercialization of microfluidic point-of-care diagnostic devices,” *Lab Chip*, vol. 12, no. 12, pp. 2118–2134, 2012.

[81] T. F. Kong *et al.*, “Enhancing malaria diagnosis through microfluidic cell enrichment and magnetic resonance relaxometry detection,” *Sci. Rep.*, vol. 5, no. June, pp. 1–12, 2015.

[82] K. El-Boubbou, “Magnetic iron oxide nanoparticles as drug carriers: Clinical relevance,” *Nanomedicine*, vol. 13, no. 8, pp. 953–971, 2018.

[83] R. K. Gilchrist, R. Medal, W. D. Shorey, R. C. Hanselman, J. C. Parrott, and C. B. Taylor, “Selective inductive heating of lymph nodes,” *Ann. Surg.*, vol. 146, no. 4, pp. 596–606, 1957.

[84] A. Ali *et al.*, “Synthesis, characterization, applications, and challenges of iron oxide nanoparticles,” *Nanotechnol. Sci. Appl.*, vol. 9, pp. 49–67, 2016.

[85] W. Wu, Z. Wu, T. Yu, C. Jiang, and W. S. Kim, “Recent progress on magnetic iron oxide nanoparticles: Synthesis, surface functional strategies and biomedical applications,” *Sci. Technol. Adv. Mater.*, vol. 16, no. 2, p. 23501, 2015.

[86] “Fe2O3 Iron Oxide Nanoparticles / Nanopowder (Alpha, 98%, 100nm, Red Color).” [Online]. Available: https://www.us-nano.com/inc/sdetail/69559. [Accessed: 24-Nov-2018].

[87] E. A. Osborne, T. M. Atkins, D. A. Gilbert, S. M. Kauzlarich, K. Liu, and A. Y. Louie, “Rapid microwave-assisted synthesis of dextran-coated iron oxide nanoparticles for magnetic resonance imaging,” *Nanotechnology*, vol. 23, no. 21, 2012.

[88] C. O. Kappe, “Controlled microwave heating in modern organic synthesis,” *Angew. Chemie - Int. Ed.*, vol. 43, no. 46, pp. 6250–6284, 2004.

[89] “Microwave Reactor (Biotage) | Materials Research Laboratory at UCSB: an NSF MRSEC.” [Online]. Available: https://www.mrl.ucsb.edu/polymer-characterization-facility/instruments/microwave-reactor-biotage. [Accessed: 05-Jan-2019].

[90] C. Leonelli and P. Veronesi, “Production of Biofuels and Chemicals with Microwave,” vol. 3, 2015.

[91] M. Wegmann and M. Scharr, *Synthesis of Magnetic Iron Oxide Nanoparticles*. Elsevier Inc., 2018.

[92] G. Cotin, S. Piant, D. Mertz, D. Felder-Flesch, and S. Begin-Colin, *Iron Oxide Nanoparticles for Biomedical Applications: Synthesis, Functionalization, and Application*. Elsevier Ltd., 2018.

[93] W. W. Wang, Y. J. Zhu, and M. L. Ruan, “Microwave-assisted synthesis and magnetic property of magnetite and hematite nanoparticles,” *J. Nanoparticle Res.*, vol. 9, no. 3, pp. 419–426, 2007.

[94] C. A. Monnier, D. Burnand, B. Rothen-Rutishauser, M. Lattuada, and A. Petri-Fink, “Magnetoliposomes: opportunities and challenges,” *Eur. J. Nanomedicine*, vol. 6, no. 4, pp. 201–215, Jan. 2014.

[95] M. Arruebo, R. Fernández-Pacheco, M. R. Ibarra, and J. Santamaría, “Magnetic nanoparticles for drug delivery,” *NanoToday*, vol. 2, no. 3, pp. 22–32, 2007.

[96] T. Neuberger, B. Schöpf, H. Hofmann, M. Hofmann, and B. Von Rechenberg, “Superparamagnetic nanoparticles for biomedical applications: Possibilities and limitations of a new drug delivery system,” *J. Magn. Magn. Mater.*, vol. 293, no. 1, pp. 483–496, 2005.

[97] B. B. Yellen *et al.*, “Targeted drug delivery to magnetic implants for therapeutic applications,” *J. Magn. Magn. Mater.*, vol. 293, no. 1, pp. 647–654, 2005.

[98] T. Kubo, T. Sugita, S. Shimose, Y. Nitta, Y. Ikuta, and T. Murakami, “Targeted delivery of anticancer drugs with intravenously administered magnetic liposomes in osteosarcoma-bearing hamsters.,” *Int. J. Oncol.*, vol. 17, no. 2, pp. 309–315, 2000.

[99] M. B. A. F. Martins, M. L. Corvo, P. Marcelino, H. S. Marinho, G. Feio, and A. Carvalho, “New long circulating magnetoliposomes as contrast agents for detection of ischemia-reperfusion injuries by MRI,” *Nanomedicine Nanotechnology, Biol. Med.*, vol. 10, no. 1, pp. 207–214, 2014.

[100] A. Skouras, K. Papadia, S. Mourtas, P. Klepetsanis, and S. G. Antimisiaris, “Multifunctional doxorubicin-loaded magnetoliposomes with active and magnetic targeting properties,” *Eur. J. Pharm. Sci.*, vol. 123, no. July, pp. 162–172, 2018.

[101] K. Watanabe, M. Kaneko, and Y. Maitani, “Functional coating of liposomes using a folate-polymer conjugate to target folate receptors,” *Int. J. Nanomedicine*, vol. 7, pp. 3679–3688, 2012.

[102] Y. Guo *et al.*, “Light/magnetic hyperthermia triggered drug released from multi-functional thermo-sensitive magnetoliposomes for precise cancer synergetic theranostics,” *J. Control. Release*, vol. 272, pp. 145–158, 2018.

[103] K. G. Paul, T. B. Frigo, J. Y. Groman, and E. V Groman, “Synthesis of Ultrasmall Superparamagnetic Iron Oxides Using Reduced Polysaccharides,” pp. 394–401, 2004.

[104] MALVERN Instruments, “Dynamic Light Scattering: An Introduction in 30 Minutes,” *DLS Tech. note MRK656-01*, pp. 1–8.

[105] R. G, F. S, and Y. A, “Two Dimensional Thin Layer Chromatographic Separation of Polar Lipids and Determination of Phospholipids by Phosphorus Analysis of Spots,” *Lipids*, vol. 5, pp. 494–496, 1970.

[106] M. Hills, C. Hudson, and P. G. Smith, “Global monitoring of the resistance of malarial parasites to drugs: statistical treatment of micro-test data,” in *Working paper No. 2.8. 5. for the informal consultation on the epidemiology of drug resistance of malaria parasites*, 1986.

[107] M. M. Gaspar *et al.*, “Targeted delivery of paromomycin in murine infectious diseases through association to nano lipid systems,” *Nanomedicine Nanotechnology, Biol. Med.*, vol. 11, no. 7, pp. 1851–1860, 2015.

[108] W. Zhang, “Nanoparticle Aggregation: Principles and Modeling,” in *Nanomaterial*, vol. 811, D. G. Capco and Y. Chen, Eds. Dordrecht: Springer Netherlands, 2014, pp. 19–43.

[109] M. L. Etheridge *et al.*, “Accounting for biological aggregation in heating and imaging of magnetic nanoparticles,” *Technology*, vol. 02, no. 03, pp. 214–228, 2014.

[110] R. Jurgons, C. Seliger, A. Hilpert, L. Trahms, S. Odenbach, and C. Alexiou, “Drug loaded magnetic nanoparticles for cancer therapy,” *J. Phys. Condens. Matter*, vol. 18, no. 38, 2006.

[111] M. Nardoni *et al.*, “Can Pulsed Electromagnetic Fields Trigger On-Demand Drug Release from High-Tm Magnetoliposomes?,” *Nanomaterials*, vol. 8, no. 4, p. 196, 2018.

[112] D. H. Kim *et al.*, “Biofunctionalized magnetic-vortex microdiscs for targeted cancer-cell destruction,” *Nat. Mater.*, vol. 9, no. 2, pp. 165–171, 2010.

[113] G. Podaru *et al.*, “Pulsed magnetic field induced fast drug release from magneto liposomes via ultrasound generation,” *J. Phys. Chem. B*, vol. 118, no. 40, pp. 11715–11722, 2014.

[114] A. Sathya, S. Kalyani, S. Ranoo, and J. Philip, “One-step microwave-assisted synthesis of water-dispersible Fe3O4 magnetic nanoclusters for hyperthermia

applications," *J. Magn. Magn. Mater.*, vol. 439, pp. 107–113, 2017.

[115] C. D. Walkey and W. C. W. Chan, "Understanding and controlling the interaction of nanomaterials with proteins in a physiological environment," *Chem. Soc. Rev.*, vol. 41, no. 7, pp. 2780–2799, 2012.

[116] J. A. Ramos Guivar *et al.*, "Magnetic, structural and surface properties of functionalized maghemite nanoparticles for copper and lead adsorption," *RSC Adv.*, vol. 7, no. 46, pp. 28763–28779, 2017.

[117] Y. Li, L. Huang, W. He, Y. Chen, and B. Lou, "Preparation of functionalized magnetic Fe3O4@Au@polydopamine nanocomposites and their application for copper(II) removal," *Polymers (Basel).*, vol. 10, no. 6, 2018.

[118] S. S. Banerjee and D. H. Chen, "Fast removal of copper ions by gum arabic modified magnetic nano-adsorbent," *J. Hazard. Mater.*, vol. 147, no. 3, pp. 792–799, 2007.

[119] M. Hedayati *et al.*, "An optimised spectrophotometric assay for convenient and accurate quantitation of intracellular iron from iron oxide nanoparticles," *Int. J. Hyperth.*, vol. 34, no. 4, pp. 373–381, 2018.

7. Appendix

Appendix I – Liposome Synthesis

Although liposome properties can change with which lipids are chosen, and in which ratios they are present, lipid vesicle production follows a generally universal procedure, divided in four main steps: lipid film formation, hydration, extrusion and washing.

Lipid Film Formation

The lipid vesicles were made by the film hydration method. DMPC, CHEMS and DSPE-PEG were dissolved in chloroform, obtaining a homogenous solution, in a round bottom flask. Said flask was then attached to a rotary evaporator, and the solvent was evaporated under vacuum until a thin film was obtained.

Dehydration-Rehydration

The film was hydrated with deionized water at 30ºC, and glass marbles were added to facilitate vesicle formation, as they gently scrapped the film off the flask's bottom and promoted hydration. This was done until there was no more film visible in the bottom. The volume was then distributed on several vials, and the flask was then washed with more water to remove any lipid residue, which was then poured into the vials as well.

These vials were then taken for freezing, and then lyophilized overnight. Having multiple vials with a portion of the volume facilitates this step. The resulting powder was rehydrated at 30ºC with HEPES buffer 7,4pH in two stages: firstly, 20% of the original liposome suspension volume was added, being vortexed repeatedly for 30 minutes. Secondly, the remaining 80% of the original suspension was added, and vortexed repeatedly for another 30 minutes. When the suspensions in the vials were observed to be homogenous, they were all added into a single vial for extrusion, and every vial was washed sequentially with the same volume of HEPES buffer, to gather any vesicles left behind during transfer to the larger vial.

Extrusion

Lipid extrusion describes the process through which the lipid suspension is filtered, by forcing it through a polycarbonate filter with a defined pore size, removing from the suspension vesicles too big for our goals. The filters used ranged from 1 to 0.1 µm (specifically 1.0, 0.8, 0.6, 0.4, 0.2 and 0.1)(***"Whatman Nuclepore"***), and the suspension would be passed up to three times through each size filter on a 10 ml extruder, to achieve minimum size dispersity.

Washing and Concentration

Using HEPES buffer, the extruded suspension was passed through a PD-10 column so the Sephadex gel would remove any small particles that were extruded along with the magnetosomes. Gravity was the driving force used to push the suspension through the column. After this washing, the magnetosomes were concentrated via ultracentrifugation (***"Beckman LM-80"***, 41171 x g, 20 min).